Earth-Science Reviews 190 (2019) 439–459

Contents lists available at ScienceDirect

Earth-Science Reviews

journal homepage: www.elsevier.com/locate/earscirev

Source and evolution of dissolved boron in rivers: Insights from boron isotope signatures of end-members and model of boron isotopes during weathering processes

Hai-Ruo Mao[a,b], Cong-Qiang Liu[a,*], Zhi-Qi Zhao[a,*,1]

[a] State Key Laboratory of Environmental Geochemistry, Institute of Geochemistry, Chinese Academy of Sciences, Guiyang 550081, China
[b] University of Chinese Academy of Sciences, Beijing 100049, China

ARTICLE INFO

Keywords:
Boron isotopes
River
Reservoirs
Mass balance model
Continental weathering
Biological cycling

ABSTRACT

The evolution of atmospheric CO_2 and the pH of the ocean can be reconstructed by the boron isotopic composition ($\delta^{11}B$) of marine carbonates, which is influenced by the $\delta^{11}B$ of the seawater. Boron (B) in the ocean is primarily affected by continental weathering through rivers. Thus, it is essential to understand the behavior of B and B isotopes in rivers and the factors affecting riverine B, which require a better understanding of sources and processes of B in river systems. This review evaluates the inventories of B reservoirs contributing to rivers and investigates the processes regulating the B isotope geochemistry of rivers.

B is widespread at the Earth's surface and shows a wide range of concentrations between reservoirs. Different reservoirs also exhibit significant variations in B isotopic compositions. Mixing and Rayleigh effects are mainly responsible for the variations in the $\delta^{11}B$ values of meteoric precipitation, which result in marine ($\delta^{11}B = +37 \pm 7‰$), anthropogenic ($\delta^{11}B = +9 \pm 10‰$), and mixing types ($\delta^{11}B = +17 \pm 13‰$) of meteoric precipitation. The contribution of B to rivers from carbonate dissolution is negligible. Marine and non-marine evaporites have distinct $\delta^{11}B$ values (marine $\delta^{11}B$: + 27 ± 9.4‰ and non-marine $\delta^{11}B$: −2 ± 8.6‰) that primarily reflect their different depositional environments. S-type granites that are tourmaline-free have an estimated $\delta^{11}B$ value of −14.2 ± 4.9‰ and a Na/B value of 140 ± 34. Non-S-type granites have a $\delta^{11}B$ value of −8.9 ± 6.7‰ and a Na/B value of 1190 ± 170. Intraplate basalts exhibit a $\delta^{11}B$ value of −5.2 ± 4.4‰ and a Na/B value of 3300 ± 770. Subduction-related basalts have a $\delta^{11}B$ value of + 0.3 ± 7.3‰ and a Na/B value of 1060 ± 830. Shale has high B contents of siliciclastic sedimentary rocks (104 ± 92 ppm). The inferred $\delta^{11}B$ values of marine and continental shales are −8‰ and −16‰, respectively. The effects of metamorphism can vary widely depending on the geologic setting and type of protolith. The $\delta^{11}B$ values of wastewater are investigated based on their industrial, agricultural, and urban sources. This inventory of B reservoirs can be useful for studies on rivers on a continental scale.

In regolith and groundwater, B isotopic fractionation mainly occurs due to water-rock interactions and the biological cycle of B, whereas adsorption on sediments leads to minor B isotopic fractionation in rivers. In groundwater, the reactive transport model reveals that the $\delta^{11}B$ value of river water is sensitive to hydrological conditions. In regolith, the steady-state mass balance model is used to predict the B isotope behavior of soil solution in different weathering regimes. In the supply-limited regime (where chemical weathering is limited by tectonic forcing), the precipitation of secondary minerals controls the variations in the $\delta^{11}B$ values of soil solution, leading to an increase in the difference in the $\delta^{11}B$ values between soil solution and parent rock ($\delta^{11}B_{diss} - \delta^{11}B_{rock}$) with lower denudation rates, whereas secondary mineral dissolution produces the opposite change in $\delta^{11}B$. In the kinetically limited regime (where chemical weathering is limited by climate), the biological cycle controls the variations in the $\delta^{11}B$ values of soil solution, and the $\delta^{11}B$ values of soil solution generally become closer to those of parent rock with higher denudation rates. The relationship between the denudation rates and $\delta^{11}B_{diss} - \delta^{11}B_{rock}$ is thus not monotonous, indicating that additional constraints are required to distinguish between the two regimes. Understanding of B isotope geochemistry of rivers can be improved by better constraints on B end-member estimates, investigation of the B isotopic fractionation caused by weathering and biological cycling in regolith, and assessment of atmospheric and biological sub-cycle.

* Corresponding author.
E-mail addresses: liucongqiang@vip.skleg.cn (C.-Q. Liu), zhaozhiqi@vip.skleg.cn (Z.-Q. Zhao).
[1] Current address: School of Earth Science and Resources, Chang'an University, Xi'an 710054, China.

https://doi.org/10.1016/j.earscirev.2019.01.016
Received 30 September 2017; Received in revised form 16 January 2019; Accepted 19 January 2019
Available online 23 January 2019

1. Introduction

Records of paleo-ocean pH can be used to reconstruct atmospheric CO_2 concentrations and to investigate paleo-ocean acidification; thus, they provide useful insights into the geochemical evolution of the atmosphere and ocean and into the global climate change (Anagnostou et al., 2016; Foster and Rae, 2016; Penman et al., 2014; Rae, 2018; Zhang et al., 2017). The boron isotopic compositions ($\delta^{11}B$) of marine carbonates are widely used for paleo-ocean pH reconstruction (Anagnostou et al., 2016; Foster, 2008; Foster and Rae, 2016; Hemming and Hanson, 1992; Henehan et al., 2016; Lemarchand et al., 2002b; Rae, 2018; Vengosh et al., 1991b), which requires a precise understanding of the secular evolution of the $\delta^{11}B$ of seawater (Gaillardet and Lemarchand, 2018; Lemarchand et al., 2000; Rae, 2018). Boron (B) in the ocean is mainly influenced by continental weathering processes through the inputs of rivers (Gaillardet and Lemarchand, 2018; Lemarchand et al., 2000, 2002b). Therefore, it is essential to understand the behavior of B and B isotopes in rivers and what factors affect the B isotopes in rivers during continental weathering. This requires a comprehensive knowledge of the reservoirs of B contributing to rivers and the processes regulating the B isotope geochemistry of rivers. Understanding these sources and processes also provides insights into the global biogeochemical cycle of B, particularly the continental B cycle.

Boron is a quintessential crustal element that is widespread in volcanic, plutonic, sedimentary, and metamorphic environments (Anovitz and Grew, 1996; Grew, 2015). Moreover, B is moderately volatile and highly soluble (Leeman and Sisson, 1996; Marschall and Foster, 2018), and it can be significantly adsorbed on clay minerals and metal oxides (Gaillardet and Lemarchand, 2018; Goldberg and Su, 2007; Lemarchand et al., 2007). B is an essential micronutrient for plants and other organisms (Blevins and Lukaszewski, 1998; Brown et al., 2002; Carrano et al., 2009). The reservoirs of B are widely distributed in the atmosphere, hydrosphere, biosphere, and lithosphere. The contents of B vary widely between reservoirs, ranging from a few ppb in rainwater to several hundred ppm in evaporites (Chetelat et al., 2009a; Leeman and Sisson, 1996; Lemarchand and Gaillardet, 2006; London et al., 1996). B has two stable isotopes, ^{10}B (19.8%) and ^{11}B (80.2%). $\delta^{11}B$ (‰) is defined as $[(^{11}B/^{10}B)_{sample}/(^{11}B/^{10}B)_{standard} - 1] \times 1000‰$, where the standard is generally NIST SRM 951. The B isotopic fractionation can be expressed as $\alpha_{A\text{-}B} = (^{11}B/^{10}B)_A/(^{11}B/^{10}B)_B$ and as $\Delta^{11}B_{A\text{-}B} = \delta^{11}B_A\text{-}\delta^{11}B_B$. In nature, the $\delta^{11}B$ values of different reservoirs exhibit significant variations (Barth, 1993; Xiao et al., 2013), ranging from −70 (Williams and Hervig, 2004) to +75‰ (Hogan and Blum, 2003). The signatures of B reservoirs are generally applicable to specific basins (Chetelat et al., 2009b; Lemarchand and Gaillardet, 2006; Liu et al., 2012; Louvat et al., 2011b, 2014; Rose et al., 2000b); however, evaluations of the B reservoirs for river systems on the continental scale are still sparse (Gaillardet and Lemarchand, 2018; Palmer and Swihart, 1996). An extensive and detailed inventory of these B reservoirs for rivers is essential for understanding the provenance constraints on the B isotopes in river water and serves as a basis of continental B cycle. With the development of analytical methods (e.g., Aggarwal et al., 2009; Gaillardet et al., 2001; Guerrot et al., 2011; Lemarchand et al., 2002a; Louvat et al., 2011a; Marschall and Monteleone, 2015; Pi et al., 2014;

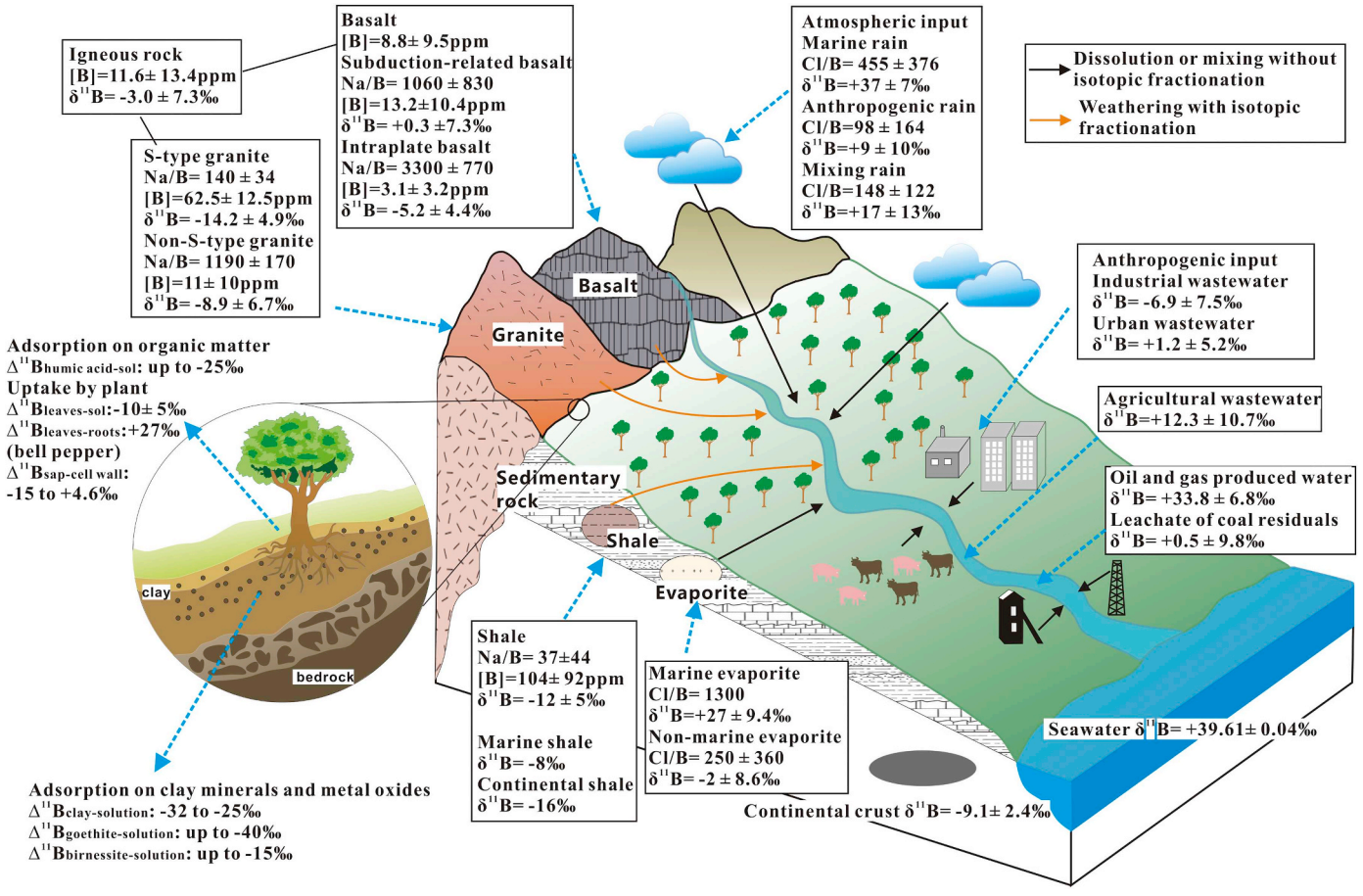

Fig. 1. Schematic of the main sources of B input into rivers and B isotopic fractionation in regolith. The uncertainty of $\delta^{11}B$ values in each reservoir is expressed as one standard deviation (1SD). The estimated $\delta^{11}B$ values of seawater and the continental crust are from Foster et al. (2010) and Marschall et al. (2017), respectively. For atmospheric inputs, see Section 2.1; for evaporites, see Section 2.3; for igneous rocks, see Section 2.4.1 (for granites, see Section 2.4.1.1 and for basalts, see Section 2.4.1.2); for shales, see Section 2.4.2; for anthropogenic inputs, see Section 2.5; and for adsorption and plant uptake, see Section 3.2.2.

Rosner et al., 2011; Tonarini et al., 1997; Wei et al., 2013; Wei et al., 2014b; Xiao et al., 1988), more accurate measurements of $\delta^{11}B$ have been reported for different types of samples, thus providing extensive data that can be used to estimate the $\delta^{11}B$ values of different sources of B in rivers.

Rivers show wide ranges of $\delta^{11}B$ values (from −10.6 to +47.3‰) and B concentrations (from 0.1 to 86.4 μmol/L); however, most rivers exhibit B concentrations that are less than 2.3 μmol/L and $\delta^{11}B$ values that vary between +2 and +20‰ (e.g., Chetelat and Gaillardet, 2005; Chetelat et al., 2009b; Farber et al., 2004; Guinoiseau et al., 2018; Lemarchand and Gaillardet, 2006; Lemarchand et al., 2000, 2002b; Liu et al., 2012; Louvat et al., 2011b, 2014; Petelet-Giraud et al., 2015; Rose et al., 2000b; Yuan et al., 2014). The mechanisms that cause this considerable variability in the B concentrations and $\delta^{11}B$ values of rivers are still poorly understood (Gaillardet and Lemarchand, 2018).

B isotopic fractionation is primarily controlled by the relative partitioning between trigonal and tetrahedral coordination (Palmer and Swihart, 1996). During water-rock interactions, the dissolution of minerals and adsorption (or coprecipitation) on clay minerals, metal (hydr)oxides, and organic matter can produce large B isotopic fractionation between rocks and fluids (e.g., Cividini et al., 2010; Lemarchand et al., 2005, 2007; Palmer et al., 1987; Rose et al., 2000b; Schwarcz et al., 1969; Spivack et al., 1987; Voinot et al., 2013; Williams et al., 2001a; Xiao and Wang, 2001). Therefore, B isotopes can be used as a sensitive tracer of water-rock interactions, particularly those in weathering of the continental surface (Cividini et al., 2010; Deyhle and Kopf, 2005; Gaillardet and Lemarchand, 2018; Lemarchand and Gaillardet, 2006; Muttik et al., 2011). Furthermore, biological cycling in regolith can lead to B isotopic fractionation (Cividini et al., 2010; Gaillardet and Lemarchand, 2018). Considering the properties of B, B isotopes in rivers have great potential for tracing rock weathering and ecosystem dynamics on a continental scale. Thus, this review aims to better understand how the B isotopes of river water change in response to weathering processes and biological cycling and to investigate the extent to which climatic and tectonic forcing affect the B isotopes of river water. Understanding the B isotopic fractionation during water-rock interactions in regolith and groundwater (e.g., Cividini et al., 2010; Gaillardet and Lemarchand, 2018; Lemarchand et al., 2012; Lemarchand and Gaillardet, 2006; Lemarchand et al., 2015) and modeling B isotopes during the weathering of regolith (Bouchez et al., 2013) can provide a good opportunity to improve our understanding of the behavior of B isotopes during weathering processes.

Here, we compile the B data of meteoric precipitation, evaporites, carbonates, igneous rocks, shales, and anthropogenic inputs and evaluate the $\delta^{11}B$ values of the B reservoirs contributing to rivers. In addition, we discuss the behavior of B in rivers and the B isotopic fractionation occurring during water-rock interactions and biological cycling in regolith and groundwater. The $\delta^{11}B$ values of the main sources of B in rivers and the B isotopic fractionation that occurs in regolith are also summarized (Fig. 1).

2. Sources of dissolved boron in rivers

2.1. Atmospheric inputs

It is necessary to evaluate the contribution of B from atmospheric input to rivers due to its potentially significant influence on rivers because river water generally has low B concentrations (Lemarchand and Gaillardet, 2006). Sea-salt aerosols, volcanic emanations, continental dust, and emissions from biomass and fossil fuel burning can contribute to atmospheric B, of which the major source is the ocean (Anderson et al., 1994; Park and Schlesinger, 2002; Schlesinger and Vengosh, 2016). The $\delta^{11}B$ values and B concentrations of meteoric precipitation range from −13 to +48‰ and from 0.1 to 69 μg/L, respectively (Anderson et al., 1994; Calabrese et al., 2011; Chetelat et al., 2009a; Chetelat et al., 2005; Fogg and Duce, 1985; Louvat et al., 2014; Martens and Harriss, 1976; Mather and Porteous, 2001; Millot et al., 2010; Miyata et al., 2000; Rose-Koga et al., 2006; Rose et al., 2000a; Rose et al., 2000b; Roux et al., 2017; Singh et al., 2014; Spivack, 1986; Xiao et al., 2007; Xiao et al., 1992; Zhao and Liu, 2010); however, our knowledge of the mechanism and influence of atmospheric B is currently incomplete.

The wide range of $\delta^{11}B$ values measured in meteoric precipitation has aroused interest in the evolution of B isotopes from seawater to meteoric precipitation. Seawater evaporation experiments conducted under open- and closed-system conditions have indicated the enrichment of ^{11}B in condensate relative to seawater and the enrichment of ^{11}B in gaseous B relative to seawater under equilibrium conditions (Chetelat et al., 2005; Xiao et al., 2007). Rose-Koga et al. (2006) inferred that the evolution of atmospheric B primarily comprises the evaporation of seawater into vapor ($\Delta^{11}B_{seawater\text{-}vapor} = +25.5‰$) and the condensation-precipitation of atmospheric vapor ($\Delta^{11}B_{vapor\text{-}rain} = -31‰$), which is modeled as a Rayleigh distillation process. This Rayleigh process (condensation) has been used to explain the $\delta^{11}B$ values of rainwater characterized by low $\delta^{11}B$ values associated with low B concentrations (Miyata et al., 2000; Roux et al., 2017). However, the large variation in the $\delta^{11}B$ values of rainwater also results from the mixing of marine sources, continental dust, and emissions from biomass and fossil fuel burning (Chetelat et al., 2009a; Chetelat et al., 2005; Millot et al., 2010; Xiao et al., 2007). For example, along the Japanese coast, the lower $\delta^{11}B$ values (−12 to +21‰) of aerosols were attributed to coal burning in North China (Sakata et al., 2013). Furthermore, the $\delta^{11}B$ values of rainwater decreased under the influence of continental dust via offshore winds in the South China Sea and Dax, France (Millot et al., 2010; Xiao et al., 2007). These data imply that atmospheric B may be sensitive to non-marine sources, even if they are located far from the sites of deposition. Based on these data and the results of experiments, we infer that precipitation derived from seawater tends to be enriched in ^{11}B relative to seawater, and we assign the marine source (noted as MS) a $\delta^{11}B$ value of +45‰ (Chetelat et al., 2005; Rose-Koga et al., 2006; Zhao and Liu, 2010).

Anthropogenic B input is another significant source of atmospheric B. Fossil fuels are commonly enriched in B: coals have a mean B content of 47 ppm, whereas oil and gasoline have lower B contents than coals (Chetelat et al., 2009a; Davidson and Bassett, 1993; Schlesinger and Vengosh, 2016; Williams and Hervig, 2004). The B isotopic fractionation that occurs during fossil fuel burning (noted as FFB) is still poorly understood. A few studies have argued that no fractionation occurs during the high-temperature combustion of coal and wood (Chetelat et al., 2005; Ruhl et al., 2014; Spivack-Birndorf and Stewart, 2006). These authors reported a $\delta^{11}B$ value of −19‰ for urban aerosol leachates that are mainly derived from coal combustion (Chetelat et al., 2009a), which is close to the average $\delta^{11}B$ value of fossil fuel (−19 ± 17‰, 1SD, from −70 to +17‰, see Supplementary Table A.5) (Williams and Hervig, 2004; Williams et al., 2001c). Despite a paucity of B data available for fossil fuel, it is reasonable to assume that the B in the products of fossil fuel burning exhibits lower $\delta^{11}B$ values. SO_4 and NO_3 are trace components of seawater that generally originate from anthropogenic sources in urban areas. Due to the heterogeneity of fossil fuel compositions, we cannot define well-constrained SO_4/B and NO_3/B ratios. To obtain a preliminary assessment of FFB, we assume that the $\delta^{11}B$ of FFB is approximately −19 ± 17‰ and that its SO_4/B and NO_3/B molar ratios are 1800 and 375, respectively (Chetelat et al., 2009a; Zhao and Liu, 2010). Biomass burning (noted as BB) has been regarded as a third significant end-member. The average $\delta^{11}B$ value of various plants in different regions is +8 ± 13‰ (1SD, ranging from −24 to +41‰) (see Supplementary Table A.4). The $\delta^{11}B$ values of plants in different regions are likely governed by the site-specific $\delta^{11}B$ values of natural reservoirs and agricultural activity (Liu et al., 2014; Rosner et al., 2011; Serra et al., 2005; Wieser et al., 2001). Moreover, recent works have indicated that leaves are enriched in ^{11}B compared to roots or stems (Geilert et al., 2015; Xu et al., 2015). Thus, the $\delta^{11}B$

values of plants are not well constrained. The SO_4/B and NO_3/B molar ratios of plants are approximately 46 and 850, respectively, based on data obtained from NIST SRM (No. 1515, 1573a, 1570a, 1547). Assuming that biomass burning is accompanied by no significant B isotopic fractionation for the same reason as coal burning and that no significant change occurs in the SO_4/B and NO_3/B ratios of plants, we assign the mean δ^{11}B value and SO_4/B and NO_3/B molar ratios of plants to those of biomass burning. Continental dust has the great potential to influence the B of rainwaters due to the large flux of dry deposition (Roux et al., 2017; Schlesinger and Vengosh, 2016). The δ^{11}B signature of continental dust is poorly constrained because it represents a combination of several sources, i.e., fertilizers, soils, carbonates, evaporates, and silicates (discussed in the following section) (Millot et al., 2010; Roux et al., 2017). Therefore, the contribution of continental dust is ignored in the present assessment.

The δ^{11}B values and B concentrations (Fig. 2a) in coastal and inland areas exhibit no marked differences. In Fig. 2b, the circled data, which have high δ^{11}B values and high Cl/B ratios, imply that this B mainly originates from a marine source. In contrast, the boxed data, which exhibit low δ^{11}B values and low Cl/B ratios, suggest that anthropogenic sources contribute considerably to meteoric precipitation. Fig. 2b demonstrates that rare locations can exhibit rainwaters characterized by high δ^{11}B values and high Cl/B ratios (marine end-member), whereas many locations show those with lower δ^{11}B values and variable Cl/B ratios due to mixed sources and/or Rayleigh process. Most of these data are distributed in a triangular area (Figs. 2c and 2d), where the values of MS, FFB and BB represent the corners. However, the circled data (Fig. 2c) that exhibit low δ^{11}B and NO_3/B ratios may be explained by continental dust, particularly silicate B-bearing minerals (Millot et al., 2010). Based on the B sources of precipitation (Fig. 2), meteoric precipitation can be classified as marine or anthropogenic. Marine meteoric precipitation is characterized by high δ^{11}B ($+37 \pm 7$‰, 1SD, n = 30) and Cl/B values (455 ± 376, 1SD, n = 21) (Supplementary Table A.3) (Chetelat and Gaillardet, 2005; Lemarchand and Gaillardet, 2006) and low NO_3/B and SO_4/B values. Conversely, anthropogenic meteoric precipitation exhibits low δ^{11}B ($+9 \pm 10$‰, 1SD, n = 41) and Cl/B values (98 ± 164, 1SD, n = 33) and high NO_3/B or SO_4/B values. The third type of rainwater probably results from the mixture of many sources and various processes (noted as mixing type); thus, this type has intermediate δ^{11}B values ($+17 \pm 13$‰, 1SD, n = 99) and wide ranges of Cl/B (148 ± 122, 1SD, n = 76), NO_3/B, and SO_4/B values.

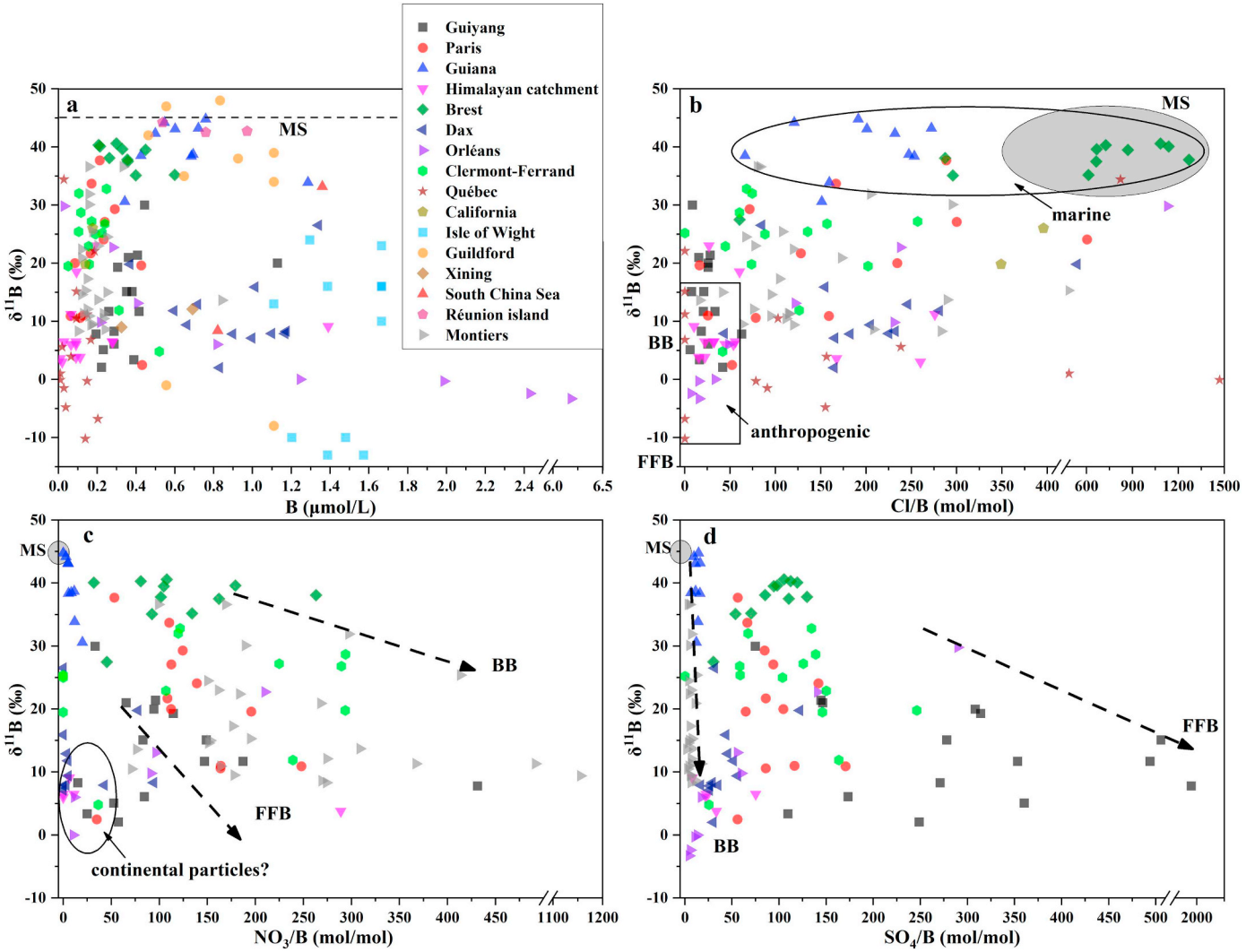

Fig. 2. Relationships between δ^{11}B values vs. B concentrations and the molar ratios of Cl/B, NO_3/B, and SO_4/B for meteoric precipitation samples from different geographic sites. (a) δ^{11}B vs. B concentration data are scattered. (b) Gray circle denotes marine source end-member (MS). The circled and boxed data denote B mainly originating from marine and anthropogenic sources, respectively. (c, d) Dashed lines denote fossil fuel burning (FFB) and biomass burning (BB) end-members. For data sources, see Supplementary Table A.1 and A.2.

2.2. Contribution of carbonates

The chemical weathering of carbonate rocks represents an important contribution to riverine dissolved loads (Amiotte-Suchet et al., 2003; Gaillardet et al., 1999; Meybeck, 1987) because the weathering rate of carbonates is faster than that of silicates (Meybeck, 1987) and carbonate rocks represent 7.8–13.4% of the continental surface (Amiotte-Suchet et al., 2003; Durr et al., 2005; Hartmann and Moosdorf, 2012). Nonetheless, the contribution of B from carbonate rocks to rivers is poorly constrained.

Boron is incorporated into carbonates from parent fluids; the B contents of carbonates increase with the B concentration and pH of a solution (Hemming et al., 1995; Hobbs and Reardon, 1999; Kitano et al., 1978; Uchikawa et al., 2015). Because the B concentrations of rivers (normally lower than 40 ppb) and fresh lakes are lower than those of seawater (4.5 ppm) (Lemarchand et al., 2002b), the B contents of continental carbonates should be much lower than those of marine carbonates, and the contribution of continental carbonates to rivers is likely negligible (Chetelat and Gaillardet, 2005; Chetelat et al., 2009b; Lemarchand and Gaillardet, 2006; Spivack and You, 1997). In marine sedimentary rocks, the high B contents of some carbonates are largely due to the presence of clay minerals that contain a substantial amount of B (Harder, 1970; Leeman and Sisson, 1996; Uppin and Karro, 2013); thus, this type of carbonate is not considered in this section. Biogenic carbonates that incorporate B from seawater generally have high B contents and higher $\delta^{11}B$ values (i.e., corals and algae have a typical B content of 50 ppm and $\delta^{11}B$ value of +25‰, as summarized by (Marschall, 2018)). Nevertheless, ancient marine carbonates have lower B contents and $\delta^{11}B$ values than modern marine carbonates, which has been attributed to the preferential removal of ^{11}B from calcite during diagenetic recrystallization (Ishikawa and Nakamura, 1993; Vengosh et al., 1991b). The inverse correlation observed between the $\delta^{11}B$ values and 1/B ratios in ancient carbonates supports this hypothesis (Gaillardet and Allegre, 1995; Spivack and You, 1997). Furthermore, deep-sea diagenesis, as verified by SEM analysis and $\delta^{13}C$, $\delta^{18}O$, Mg/Ca, and Sr/Ca data (Kozdon et al., 2013; Regenberg et al., 2007), results in B loss (Coadic et al., 2013; Edgar et al., 2015). The variations in B in ancient seawater resulting from enhanced continental weathering could also result in the lower $\delta^{11}B$ values or B contents of marine carbonates (Joachimski et al., 2005; Paris et al., 2010a). Even if marine biogenic carbonates are well preserved, those that underwent diagenetic alteration following tectonic uplift, especially ancient carbonates, could have lower B contents (Joachimski et al., 2005). Regardless of the exact mechanism, the mean B concentration of inorganic carbonates is 2.6 ± 4.2 ppm (1SD, n = 109, Supplementary Table A.6).

The Ca/B molar ratios of carbonates, which are used to calculate the contributions of dissolved boron from carbonate dissolution in river water, range from 10,000 to 20,000 (Lemarchand and Gaillardet, 2006; Rose et al., 2000b), suggesting that the contribution of B from carbonates was mainly less than 5% (Chetelat and Gaillardet, 2005; Chetelat et al., 2009b; Lemarchand and Gaillardet, 2006; Rose et al., 2000b). Based on the majority of data obtained from carbonates and rivers, we assume that the contribution of B from carbonate dissolution to rivers is negligible (Gaillardet and Lemarchand, 2018).

2.3. Dissolution of evaporites

Although evaporites account for a small percentage of outcrops (0.1–0.3%), their rapid dissolution rate and very high B contents (which can reach up to 2000 ppm) may lead to a large contribution of dissolved B to rivers (Durr et al., 2005; Hartmann and Moosdorf, 2012; Lemarchand and Gaillardet, 2006; London et al., 1996; Meybeck, 1987). The highly variable B contents in evaporite minerals and the obvious distinction between the mean $\delta^{11}B$ values of marine and non-marine evaporites (Fig. 3) complicate the evaluation of their B contributions (London et al., 1996; Rose et al., 2000b; Swihart et al., 1986). Cl/B molar ratios are normally used to assess the contributions of evaporites to rivers (Chetelat et al., 2009b; Lemarchand and Gaillardet, 2006). The Cl/B molar ratio of marine evaporites is considered to be similar to that of seawater (ca. 1300; Vengosh et al., 1991a), and it was proposed to be ca. 1000 by Lemarchand and Gaillardet (2006). However, it is difficult to estimate a well-constrained Cl/B ratio for non-marine evaporites, given the mixing of multiple sources and their variety of depositional settings (Qi et al., 1993; Vengosh et al., 1995; Xiao et al., 1999). Thus, the Cl/B ratio in non-marine evaporites is

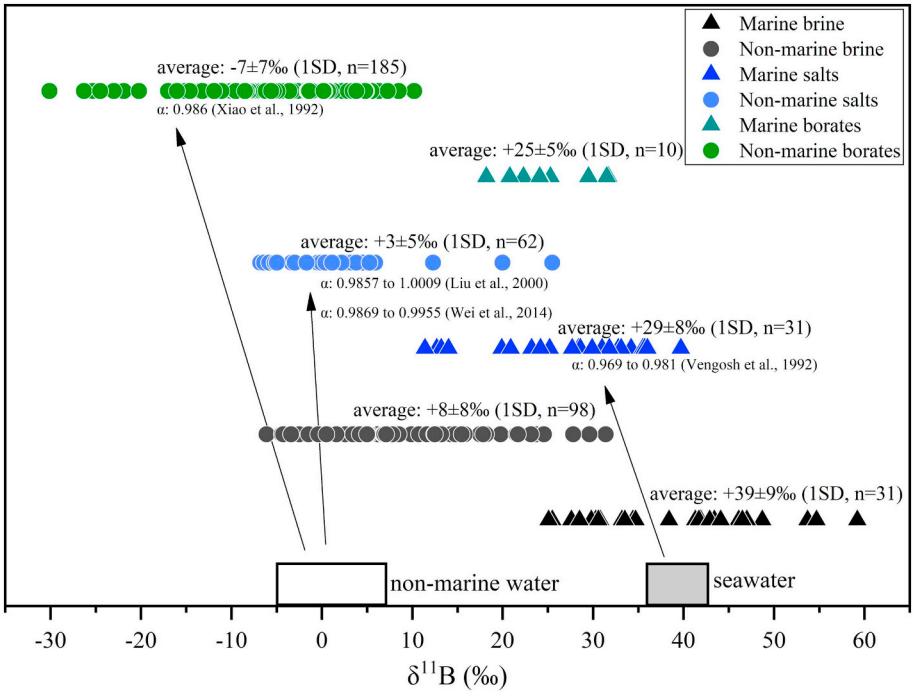

Fig. 3. Variations in the $\delta^{11}B$ values of brine, salts and borates produced by the evaporation of seawater and non-marine water. Salts represent halite and/or gypsum and borates denote borate minerals, such as borax, ulexite, colemanite, and boracite. The fractionation factors reported in the literature are $\alpha_{borate\text{-}brine}$: 0.986(Xiao et al., 1992); $\alpha_{salt\text{-}brine}$: 0.9857–1.0009 (Liu et al., 2000); $\alpha_{salt\text{-}brine}$: 0.9869–0.9955 (Wei et al., 2014a); and $\alpha_{salt\text{-}brine}$: 0.969–0.981 (Vengosh et al., 1992). For data sources, see Supplementary Tables A.7 and A.8.

tentatively assumed to be 250 ± 360 (1SD, n = 50) based on the data compiled from Vengosh et al. (1995) and Zheng and Liu (2009) and references therein. This ratio is higher than that of 140, which was obtained in the Changjiang River (Chetelat et al., 2009b). A SO_4/B value of 8000 is also used to assess the B contributions of evaporites (Chetelat et al., 2009b; Lemarchand and Gaillardet, 2006); however, the coexistence of gypsum and halite in evaporites probably causes an overestimation of the B content. Thus, SO_4/B ratios can be used for gypsum-rich evaporites.

The incorporation of B from brine into salts may be explained by two mechanisms: (1) trapping in fluid inclusions and (2) incorporation in the mineral lattice (Vengosh et al., 1992). The first mechanism indicates that the $\delta^{11}B$ values of halite are similar to those of their parent solution, with the minor coprecipitation of $CaSO_4$ ([Ca] < 1g/L) (Fan et al., 2015; Liu et al., 2000; Paris et al., 2010b); in contrast, the second mechanism indicates that salts selectively uptake ^{10}B associated with the coprecipitation of $CaSO_4$, $MgSO_4$, or $CaCO_3$ (Hemming et al., 1995; Liu et al., 2000; Noireaux et al., 2015; Vengosh et al., 1992), thus decreasing the $\delta^{11}B$ values of salts ($\alpha_{salt\text{-}brine}$: 0.969–0.981) (Vengosh et al., 1992).

The distinct differences between the $\delta^{11}B$ values of marine and non-marine borate minerals are attributed to their different sources of B (Barth, 1993; Bassett, 1990; Swihart et al., 1986). Furthermore, the $\delta^{11}B$ values of the borates in the same depositional environment depend on not only the mineralogy of borates (Oi et al., 1989) but also the pH of the brine during the precipitation of borates (Palmer and Helvaci, 1995; Palmer and Helvaci, 1997). Despite the diversity of borates and salts, there are similar patterns in the $\delta^{11}B$ values of evaporites between these two sources: (1) the $\delta^{11}B$ values of marine brine, salts, and borates are usually higher than those of their non-marine counterparts; and (2) the average $\delta^{11}B$ values in these two environments decrease in the same order of brine > salts and borates (Fig. 3). Additionally, because most borate minerals in evaporites are soluble, the B entering rivers from evaporites should be the sum of that from salts and borates. Nevertheless, because of the higher solubility of halite than that of borates (ulexite and colemanite) and the various proportions of salts to borates in evaporites, the contribution of B from the dissolution of salts and borates to rivers is unclear. We tentatively assume that the B entering rivers from the dissolution of salts is equal to that of borates. The $\delta^{11}B$ value of modern seawater is +39.6‰, which could be representative of the $\delta^{11}B$ value of marine evaporites considering the near-uniform composition of seawater, whereas the varying $\delta^{11}B$ values of ancient seawater (e.g., Joachimski et al., 2005; Lemarchand et al., 2000; Paris et al., 2010b) and diagenesis (Smith and Medrano, 1996) would lead to a different $\delta^{11}B$ value of marine evaporites; thus, the $\delta^{11}B$ value of marine evaporites is proposed to be +27 ± 9.4‰ (the mean $\delta^{11}B$ value of the average values of marine salts and borates; Fig. 3). Likewise, the $\delta^{11}B$ value of non-marine evaporites is presumed to be −2 ± 8.6‰ (i.e., the mean $\delta^{11}B$ value of the average values of non-marine salts and borates), which falls within the range of the mean $\delta^{11}B$ value, i.e., −4 to +2‰ (Chetelat et al., 2009b; Wang et al., 2001).

2.4. Silicate weathering

Silicate rocks include igneous rocks (13.0–14.1% of the continental surface), metamorphic rocks (4.1–13.0% of the continental surface), and sedimentary rocks (e.g., shale and sandstone account for 11.4% and 4.9% of the continental surface, respectively) (Durr et al., 2005; Hartmann and Moosdorf, 2012). It is commonly accepted that the weathering of silicate rocks contributes most of the dissolved B to rivers (Chetelat et al., 2009b; Lemarchand and Gaillardet, 2006; Liu et al., 2012; Rose et al., 2000b). Nonetheless, it is difficult to characterize the contribution of silicate weathering to the dissolved B in rivers due to the diverse compositions and different weathering rates of silicate minerals; thus, previous studies have usually considered the contribution of silicate weathering to represent the remainder following the correction of other source contributions (e.g., atmosphere, evaporites, and anthropogenic input) (Lemarchand and Gaillardet, 2006; Liu et al.,

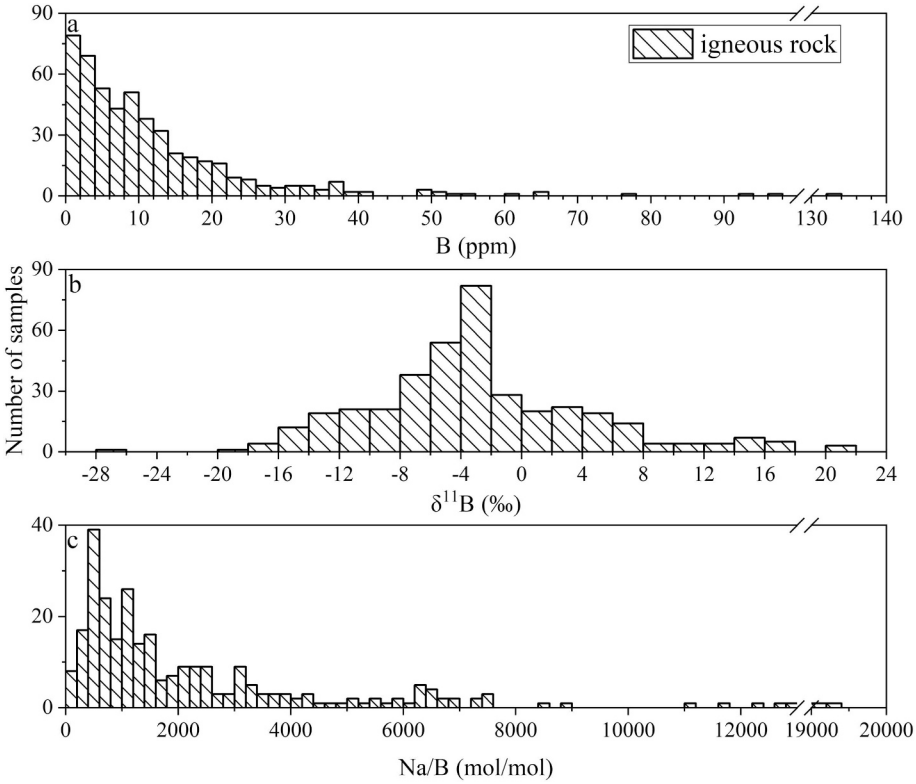

Fig. 4. Histograms of B contents, $\delta^{11}B$ values, and Na/B molar ratios of igneous rocks. For data sources, see Supplementary Table A.10.

2012; Rose et al., 2000b). There are noticeable differences between the B contents of sedimentary and igneous rocks; for instance, the abundance of B in shale is usually higher than that in igneous rock (Leeman and Sisson, 1996). Hence, it is necessary to distinguish the contributions of B from different types of silicate rocks.

2.4.1. Igneous rock

In igneous rocks (excluding tourmaline-bearing rocks), B contents are generally less than 10 ppm, and their $\delta^{11}B$ values cluster between −8 and 0‰ (Figs. 4a and 4b). Igneous rocks have a similar mean B content of 11.6 ± 13.4 ppm (1SD, n = 506) compared to the continental crust and a higher mean $\delta^{11}B$ value of −3.0 ± 7.3‰ (1SD, n = 383) compared to the continental crust (Supplementary Table A.9). Na/B molar ratios are used to discriminate between the contributions of igneous and sedimentary rock in river water, as Na is conservative and igneous and sedimentary rocks have different Na contents. These vast ranges of Na/B and $\delta^{11}B$ (Figs. 4b and 4c) reflect that the B in igneous rocks is likely derived from various sources and influenced by different processes. Therefore, it is necessary to study different types of igneous rocks. The two most common and distinct igneous rocks, i.e., granite (5.7–7.2% of the continental surface) and basalt (3.5–5.8% of the continental surface) (Durr et al., 2005; Hartmann and Moosdorf, 2012), are selected to discuss the B behavior of igneous rocks. The $\delta^{11}B$ values, B contents, and Na/B ratios of basalts and granites are shown in Fig. 5.

2.4.1.1. Granite. Granite is the main reservoir of B in igneous rocks because B is concentrated in the melt by crystal fractionation (London et al., 1996). S-type granites are commonly considered the most "fertile" granites because B is released from the anatexis of B-rich metasedimentary rocks (London et al., 1996). Tourmaline is a weather-resistant borosilicate mineral and is commonly found in S-type granite. Thus, the influence of tourmaline should be carefully eliminated from S-type granite when assessing the effect of granite weathering on river water compositions. Granites can be divided into two groups: non-S-type granites (i.e., I-, A- and M-types) (Figs. 5a to 5c) and S-type granites (S-I-A-M classification based on Winter, 2014).

The various compositions and metamorphic histories of (meta-)sedimentary protoliths result in different types of tourmaline, which can be derived from melt or exsolved fluid (Jiang and Palmer, 1998; Trumbull and Slack, 2018) and lead to large variations in the $\delta^{11}B$ values of tourmaline in granites, ranging from −29.9 to +0.8‰ (Chaussidon and Albarède, 1992; Jiang and Palmer, 1998). Thus, it is complicated to exclude tourmaline from S-type granite. To simplify this evaluation, S-type granites are presumed to form by melting (meta-)

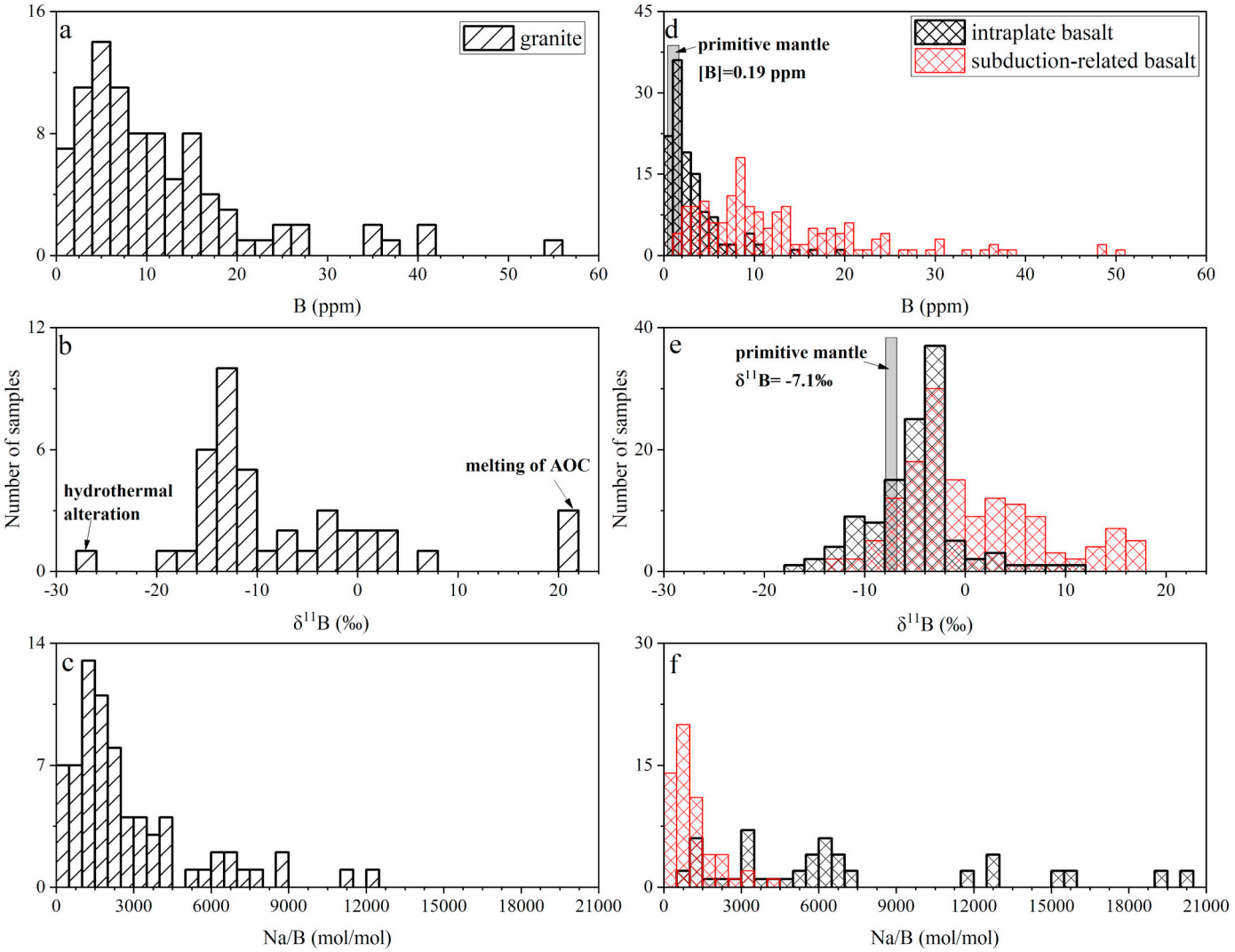

Fig. 5. Histograms of B contents, $\delta^{11}B$ values, and Na/B molar ratios of granite and basalt. a to c represent granites, and d to f represent basalts. The B content and $\delta^{11}B$ value of the primitive mantle are estimated by Marschall et al. (2017). The basalts show an average B content of 8.8 ± 9.5 ppm (1SD, n = 292) and a mean Na/B ratio of 3300 ± 4200 (1SD, n = 108). For data sources, see Supplementary Tables A.11 and A.12.

sedimentary protoliths (London et al., 1996) that are assumed to have the same composition and metamorphic history and only experience magmatic differentiation. The $\delta^{11}B$ value of S-type granite (removing tourmaline) can be estimated by excluding the $\delta^{11}B$ value of the melt crystalized into tourmaline. The formation of tourmaline from melt and fluids can generally be modeled as Rayleigh processes (Drivenes et al., 2015; Marschall et al., 2009; Siegel et al., 2016; Trumbull et al., 2013). The $\delta^{11}B$ value of the residual melt is estimated to be −13.3‰ at 650°C and −15.1‰ at 500°C (methods see Supplementary B.1). After excluding the contribution of tourmaline, the $\delta^{11}B$ value and B content of S-type granite are estimated to be −14.2 ± 4.9‰ and 62.5 ± 12.5 ppm, respectively (methods see Supplementary B.1). The Na/B molar ratio of S-type granite is 140 ± 34 based on the Na content of the S-type granite (2.5%) (Winter, 2014).

This non-S-type granite originates from producing melt by melting the mantle ($\delta^{11}B$ of −7.1‰) or crustal material ($\delta^{11}B$ of −9.1‰) (Supplementary Table A.9) that then experiences fractional crystallization, magma mixing and assimilation. Generally, B isotopes fractionate slightly during anatexis and magmatic differentiation, implying that the $\delta^{11}B$ values of non-S-type granite are similar to those of source rocks (Kaliwoda et al., 2011; Romer et al., 2014a; Trumbull and Slack, 2018). However, non-S-type granite can be contaminated by exsolved fluids from country rock or meteoric fluids that are enriched in ^{11}B (Drivenes et al., 2015; Kaliwoda et al., 2011; Trumbull et al., 2013; Zhao et al., 2011). The various influences of magma mixing and of assimilation can lead to the abnormal $\delta^{11}B$ values of granite (Cividini et al., 2010; Lemarchand et al., 2012; Romer et al., 2014a) (Fig. 5b). After excluding outliers, we can assign a mean $\delta^{11}B$ value of −8.9 ± 6.7‰ (1SD, n = 36) (Supplementary Table A.11) to the non-S-type granite, which is similar to the $\delta^{11}B$ values of the mantle and continental crust. The B contents of granites range from 1 to 55 ppm and cluster between 6 and 8 ppm (Fig. 5a), reflecting that granites in different environments display similar enriched patterns. Therefore, we assume that the average B content of 11 ± 10 ppm (1SD, n = 86) in the non-S-type granite represents an end-member composition. The Na/B ratios of non-S-type granites cluster around 1300 (Fig. 5c), which is similar to the calculated Na/B of 1190 ± 170 (Supplementary B.1), whereas their average Na/B value is 2200 ± 1670 (1SD, n = 67) (excluding those over 7000) because some samples have relatively low B contents (< 5 ppm). Therefore, the Na/B value of non-S-type granites is estimated to be 1190 ± 170.

2.4.1.2. Basalt. B and B isotopes in subduction-related and intraplate basalts are topics of great interest because they are sensitive tracers of water-rock processes and crustal cycling (de Hoog and Savov, 2018; Leeman and Sisson, 1996; Marschall, 2018; Palmer, 2017). Intraplate basalts generally have lower B contents than subduction-related basalts (Leeman and Sisson, 1996; Li et al., 2016; Ryan et al., 1996), but the discrepancy between $\delta^{11}B$ values of these basalts is unclear. Intraplate basalts are primarily derived from the mantle, and their B contents and isotopes are chemically similar to those of mid-ocean ridge basalt (MORB) or oceanic island basalt (OIB). Unaltered MORB shows a wide range of $\delta^{11}B$ values from −12 to 0‰ (Ishikawa and Nakamura, 1992; Marschall, 2018; Roy-Barman et al., 1998). However, the global range of uncontaminated MORB (with low Cl/K), whose heterogeneity is identified by radiogenic isotopes and trace elements (including depleted and enriched MORB), shows no significant variations in $\delta^{11}B$, suggesting that pristine MORB has homogeneous $\delta^{11}B$ values (Marschall et al., 2017). Thus, the estimated B content and $\delta^{11}B$ value of depleted MORB-source mantle are 0.077 ppm and −7.1 ± 0.9‰, respectively (Marschall et al., 2017). Furthermore, the assimilation of seawater (or brine) or seawater-altered materials can significantly increase the $\delta^{11}B$ value of MORB (Chaussidon and Jambon, 1994; Marschall et al., 2017). OIB shows a wide range of $\delta^{11}B$ values from −17 to +12‰ (Supplementary Table A.12), which is largely influenced by the assimilation of crustal materials altered by seawater or hydrothermal fluids during magma ascent (Brounce et al., 2012; Genske et al., 2014; Marschall, 2018). In contrast, some studies have suggested that the $\delta^{11}B$ excursion of OIB from MORB mainly reflects the mixing of primitive mantle with recycled subducted materials (Kobayashi et al., 2004; Li et al., 2016; Tanaka and Nakamura, 2005; Turner et al., 2007). Intraplate basalts generally exhibit low B contents (average 3.1 ± 3.2 ppm, 1SD, n = 120) and $\delta^{11}B$ values (average −5.2 ± 4.4‰, 1SD, n = 115) (Figs. 5d and 5e, Supplementary Table A.12). The mean Na/B molar ratio of intraplate basalts is 3300 ± 770, which is calculated using the mean contents of Na_2O (2.9 ± 0.7%) (Farmer, 2014) due to the paucity of Na/B data.

B is highly depleted in the mantle and strongly enriched in subducted sediments, altered oceanic crust (AOC), and the serpentinized mantle; hence, the B values of subduction-related basalts are largely regulated by the various sources of B-rich fluids, dehydration processes, and the structure of the subduction zone (de Hoog and Savov, 2018; Konrad-Schmolke and Halama, 2014; Manea et al., 2014). Subducted sediments exhibit wide variations in their B contents (ca. 50 to 150 ppm) and $\delta^{11}B$ values (ca. −13 to +5‰) (Ishikawa and Nakamura, 1993; Marschall, 2018; Plank, 2014; Tonarini et al., 2011) and are estimated to have weighted average values of [B] = 53 ppm and $\delta^{11}B$ = −1.6‰ (Leeman and Sisson, 1996). AOC shows variable B contents (from 1 to 104 ppm, mean [B] = 5.2 ppm) and $\delta^{11}B$ values (from −4 to +25‰, mean $\delta^{11}B$ = +3.4‰) (Marschall, 2018; Smith et al., 1995). Most ^{11}B-rich fluids are released from AOC and sediments at shallow depths during the early stages of dehydration (de Hoog and Savov, 2018; Scambelluri and Tonarini, 2012; Tonarini et al., 2011). Serpentinites have very high B contents (up to 91 ppm) and high $\delta^{11}B$ values of ca. +5 to +40‰ (Boschi et al., 2013; Boschi et al., 2008; Harvey et al., 2014b; Spivack and Edmond, 1987; Vils et al., 2009). Serpentinites mainly deliver ^{11}B-rich fluids at deep depths; however, the B isotopic fractionation during the dehydration of serpentinite remains unclear (Harvey et al., 2014a; Metrich and Deloule, 2014; Scambelluri and Tonarini, 2012). A combined thermodynamic-geochemical model was developed, which integrates mass balance and B isotopic fractionation with the thermal geometry of the subduction zone (Konrad-Schmolke and Halama, 2014; Konrad-Schmolke et al., 2016; Marschall et al., 2007; Marschall et al., 2006; Prigent et al., 2018). Subduction-related basalts have an average B content of 13.2 ± 10.4 ppm (1SD, n = 165), an average $\delta^{11}B$ value of +0.3 ± 7.3‰ (1SD, n = 148), and an average Na/B value of 1060 ± 830 (1SD, n = 67) (Supplementary Table A.12).

2.4.2. Sedimentary rock

Silicate minerals are commonly found in siliciclastic sedimentary rocks, including shale, sandstone, and conglomerates. Here, shales refer to all fine-grained siliciclastic sedimentary rocks. Shales account for a large portion of the continental surface (Durr et al., 2005) and comprise most of sedimentary rocks (Ilgen et al., 2017). Generally, shales have the highest B contents of all siliciclastic sedimentary rocks, because clay minerals, which have high B contents due to adsorption, are the major constituents of shales (Leeman and Sisson, 1996). Thus, shale may be an adequate representative for assessing the contribution of B from the silicate minerals of sedimentary rocks.

B in shale is primarily derived from the clay minerals adsorbed from depositional environments (Cody, 1970; Harder, 1970), organic matter (Williams et al., 2001c; Williams et al., 2013), and continental and marine sediments (Leeman and Sisson, 1996). Shale can be simply classified as marine or continental shale based on its depositional environment (Cody, 1970), where seawater and freshwater generally have distinct B contents and $\delta^{11}B$ values (Lemarchand et al., 2002b). Buried organic matter (e.g. coal and kerogen), which is enriched in B (commonly 50–200 ppm), will release ^{10}B-enriched fluids with increasing temperature during maturation, but the $\delta^{11}B$ values of organic-derived fluids are scarce (−12 to +16‰, mean $\delta^{11}B$ = −1.5‰, n = 4) (Clauer et al., 2018; Williams and Hervig, 2004; Williams et al., 2001c). Marine

sediments show variable B contents and $\delta^{11}B$ values (see Section 2.4.1.2). Soils are a major source of continental sediments, showing variable B contents (ca. from 10 to 100 ppm) and $\delta^{11}B$ values (ca. from −30 to +10‰) (Gaillardet and Lemarchand, 2018; Leeman and Sisson, 1996; Lemarchand et al., 2012; Noireaux et al., 2014; Spivack et al., 1987). The B contents in shale are generally controlled by adsorption, diagenesis, and metamorphism. The differences between the B contents of seawater and freshwater can result in higher B contents of marine shale than those of continental shale, whereas factors such as mineralogy, grain size, organic matter, and metamorphism can change the B contents of shale (Cody, 1970; Engle et al., 2016; Harder, 1970; Williams et al., 2007). In addition, the depositional environments of sedimentary basins can vary widely (e.g., Romer et al., 2014b). The B contents of shale (Fig. 6a) cluster around 80 ppm, suggesting that the difference between the B contents of continental and marine shale is small. Our mean B content of shales is 104 ± 92 ppm (1SD, n = 181) (Supplementary Table A.13), which is similar to previous estimates of ca. 100 ppm (Harder, 1970; Shaw and Bugry, 1966; Spivack et al., 1987; Wedepohl, 1971). The mean Na/B molar ratio of shales is 37 ± 44 (1SD, n = 134), which is not far from the Na/B value of 50 determined based on the mean Na content of shales (Na_2O: 1.5%) (Boggs, 2011). It is still necessary to briefly summarize the other factors that control the B contents in shales.

Adsorption studies have suggested that factors such as pH, clay mineralogy, grain size, temperature, and the B content of water can influence adsorption, e.g., B adsorption increases with increasing pH (with maximum adsorption occurring at pH = 8–10), adsorption occurs in the order of illite > montmorillonite > kaolinite, and the higher B contents of a solution are associated with higher amounts of adsorption (e.g., Goldberg, 1997; Goldberg and Glaubig, 1986; Goldberg and Su, 2007; Keren and Mezuman, 1981; Keren and Talpaz, 1984; Mattigod et al., 1985; Palmer et al., 1987; Singh, 1971). Furthermore, diagenesis also comprises two stages: the desorption of B from clays transferred into pore fluids (the amount of adsorbed B is negligible when T > 120°C) (Leeman and Sisson, 1996; You et al., 1996) and the incorporation of B into the interlayers and tetrahedral sites of clay minerals (Williams and Hervig, 2002; Williams et al., 2001a). The B contents in clay minerals can approach equilibrium with pore fluids (Williams and Hervig, 2002; Williams et al., 2001a; Williams et al., 2001b); thus, argillaceous sediments do not experience significant B loss during diagenesis (Ishikawa and Nakamura, 1993). Moreover, during diagenesis, pore fluids can be influenced by the dissolution of evaporites and the maturation of organic matter (Ilgen et al., 2017; Williams et al., 2001b; Williams et al., 2013).

The $\delta^{11}B$ values of shale (Fig. 6b) exhibit a possible bimodal distribution, with apparent peaks near −16 and −8‰ and an average $\delta^{11}B$ value of −12.0 ± 5‰ (1SD, n = 87). However, this pattern is provisional considering the paucity of $\delta^{11}B$ data. Clay minerals, the depositional environment, diagenesis, and metamorphism are essentially responsible for variations in the $\delta^{11}B$ values of shales. In general, illite-rich clays have lower $\delta^{11}B$ values than smectite-rich clays (Ishikawa and Nakamura, 1993; Spivack et al., 1987), likely due to the preference of ^{10}B to enter the tetrahedral sites of illite/smectite during illitization (Williams and Hervig, 2002; Williams et al., 2001a). The $\delta^{11}B$ values of pore fluids and clay-solution isotope fractionation play important roles in controlling the $\delta^{11}B$ values of sediments as a result of

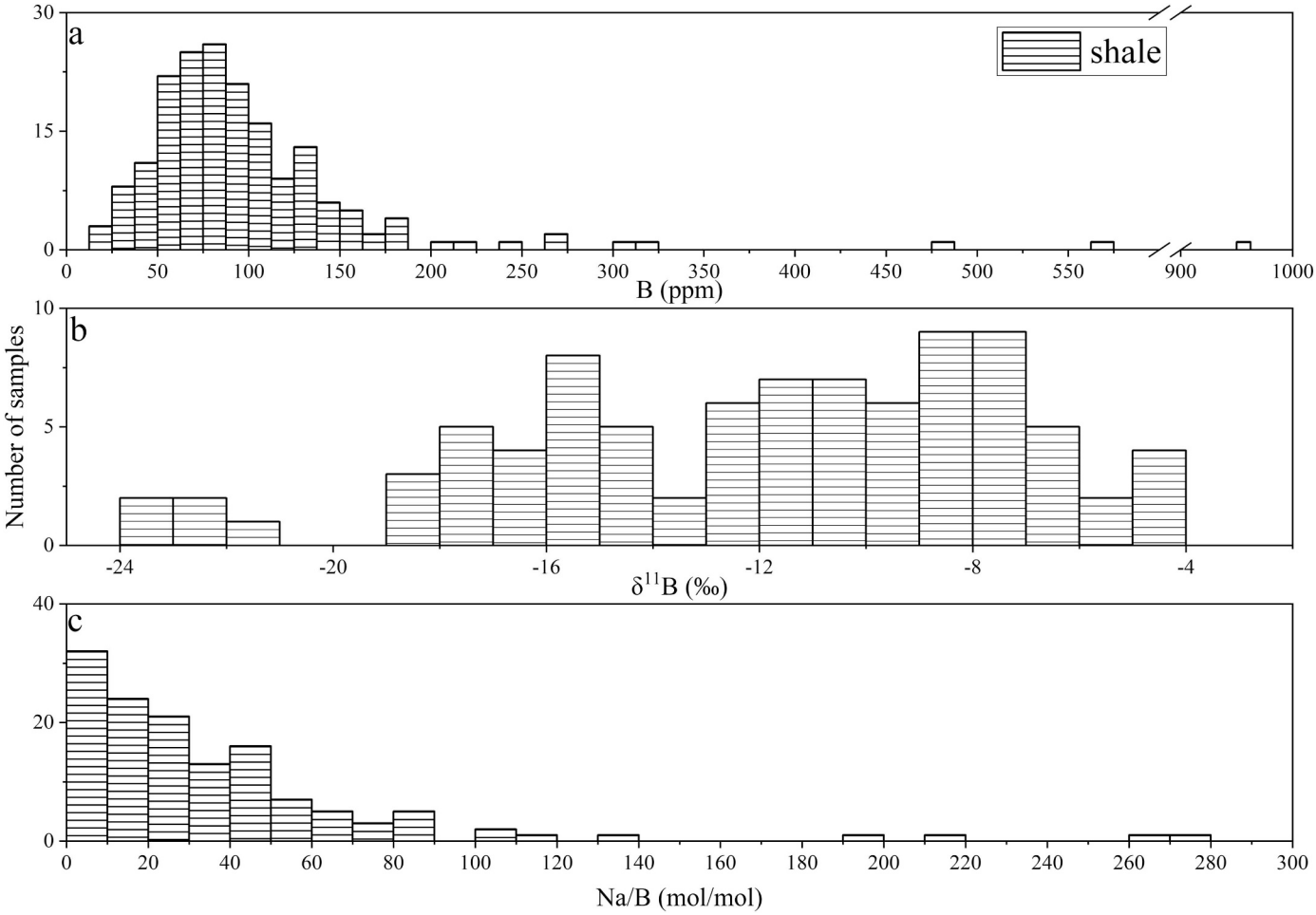

Fig. 6. Histograms of B concentrations, $\delta^{11}B$ values, and Na/B molar ratios of shale. For data sources, see Supplementary Table A.13.

B adsorption. Pore fluids are commonly derived from rivers, seawater, and organic-derived fluids. B isotopic fractionation between clay minerals/sediments and fluids depends mainly on the pH of the solution at low temperatures (Lemarchand et al., 2015; Palmer et al., 1987; Xiao and Wang, 2001). The adsorption of B from seawater on clay minerals leads to $\Delta^{11}B_{clay\text{-}seawater}$ values of −32‰ to −25‰ at pH values of 6.8–8 (Palmer et al., 1987; Spivack et al., 1987). The $\Delta^{11}B_{sediment\text{-}water}$ values of rivers vary widely, ranging from −31.2 to −5.8‰ (pH = 7.5 ~ 9.5); however, fractionation probably does not result from adsorption in rivers (Chetelat et al., 2009b; Liu et al., 2012; Rose et al., 2000b). Thus, the differences between the $\delta^{11}B$ values of marine and river sediments probably reflect the combined effects of adsorption and the mineralogy of sediments. Marine sediments have higher $\delta^{11}B$ values (average $\delta^{11}B$ = −1.6‰ (Leeman and Sisson, 1996)); in contrast, river sediments show lower $\delta^{11}B$ values (average $\delta^{11}B$ = −11.3‰, ranging from −18.8 to −3.5‰) (Chetelat et al., 2009b; Lemarchand and Gaillardet, 2006; Pennisi et al., 2009; Spivack et al., 1987). The observed fractionation during late diagenesis and metamorphism (T > 250°C) is $\Delta^{11}B_{diagenesis}$ = −19‰ at 200°C and −15‰ at 300°C (Williams et al., 2001a; Williams et al., 2001b). The $\Delta^{11}B_{diagenesis}$ = −22.7‰ at 125°C, which is based on the empirical equation (Williams et al., 2007) and indicates the wide variation in fractionation (~7‰ between 125°C and 300°C) occurring during diagenesis and metamorphism. Diagenesis and organic-derived B can lead to the lower $\delta^{11}B$ values of shales relative to those of sediments (Marschall, 2018). Nevertheless, the extent of the decrease in the $\delta^{11}B$ values of shales is different. We thus tentatively designate the $\delta^{11}B$ values of the continental and marine shale end-members as −16‰ and −8‰, respectively.

2.4.3. Metamorphic rock

Many factors can regulate the behavior of B during metamorphism, such as the composition of the protolith, the P-T-t path, the composition of the fluid, and the stability of the minerals that host B (Leeman and Sisson, 1996). Inferences about the behavior of B and its isotopes during metamorphism that are drawn from comparisons between metamorphic rocks and an average protolith have yielded varying results, due to the large variability in the $\delta^{11}B$ values of protoliths (Romer and Meixner, 2014). Despite the diversity of metamorphic processes and protoliths, some general inferences can be drawn.

Contact metamorphism generally occurs adjacent to igneous intrusions that may exsolve hydrothermal fluids into the country rock. Hydrothermal fluids can transfer B from an intrusion into the country rock. Thus, if igneous intrusions expel B-rich fluids, the contact aureoles in the country rock may exhibit elevated B contents and even tourmalinization (Leeman and Sisson, 1996; Woodford et al., 2001). Generally, these fluids are enriched in ^{11}B relative to the original magma (Drivenes et al., 2015; Jiang and Palmer, 1998; Kaliwoda et al., 2011; Smith and Yardley, 1996; Trumbull et al., 2013; Trumbull et al., 2008; Zhao et al., 2011), and the $\delta^{11}B$ values of fluids vary widely; for instance, fluids from marine evaporites have higher $\delta^{11}B$ values of +20‰ (Lambert-Smith et al., 2016) and fluids from non-marine sedimentary rocks have lower $\delta^{11}B$ values of −13‰ (Jiang, 2001; Marschall and Jiang, 2011).

Regional metamorphism affects boron more subtly than contact metamorphism due to its more gradual thermal gradients and lower water-rock ratios. Moreover, the nature of the protolith and the presence of B-bearing minerals and their P-T stability exert key influences on B and its isotopic geochemistry (Leeman and Sisson, 1996; Romer and Meixner, 2014). Low-grade metamorphism causes the overall loss of B and minor B isotopic fractionation to lower $\delta^{11}B$ values, which depends on the relative contributions of B in the mineral lattice and B on the mineral surface (Romer and Meixner, 2014). During high-grade metamorphism, devolatilization reactions preferentially remove ^{11}B from B-bearing minerals, principally mica and chlorite, thus resulting in the lower $\delta^{11}B$ values and B concentrations of the residual rocks (Bebout, 2007; Bebout and Nakamura, 2003; Benton et al., 2001; Marschall et al., 2007; Moran et al., 1992; Nakano and Nakamura, 2001; Peacock and Hervig, 1999; Wunder et al., 2005). In addition, this released boron may be sequestered in the rock (probably representing a small fraction of the B in newly formed tourmaline) (e.g., Nakano and Nakamura, 2001; Romer and Meixner, 2014).

2.5. Anthropogenic inputs

With increasing human activities, the inputs of anthropogenic B into rivers have increased up to 0.65 Tg B/yr, thus strongly influencing the B inventory in rivers (Schlesinger and Vengosh, 2016). The major

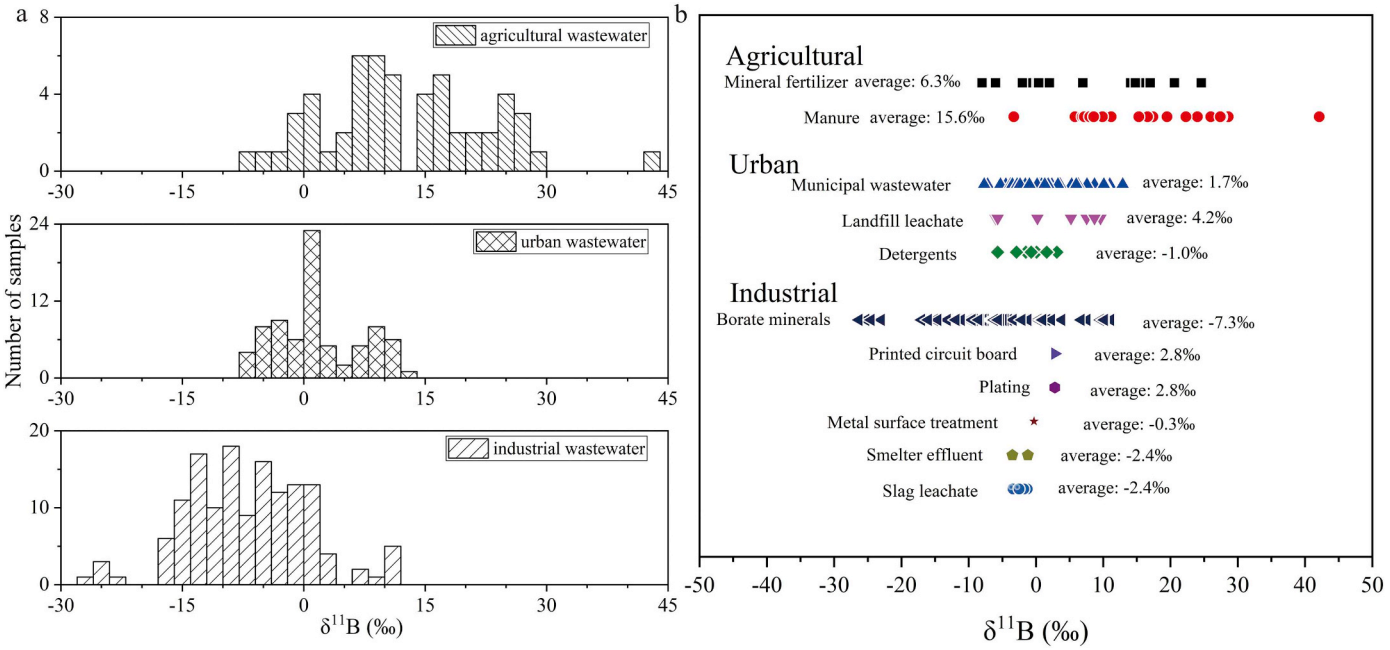

Fig. 7. (a) Histograms of the $\delta^{11}B$ values of industrial, urban, and agricultural wastewater; (b) $\delta^{11}B$ values of different subgroups of wastewater. For data sources, see Supplementary Tables A.14 and A.15.

anthropogenic inputs into rivers stem from the exploitation of oil and combustion of coal, industrial and urban effluents, and agricultural wastewater.

The B concentrations of coal vary widely from 10 to 1000 ppm, with a mean B concentration of approximately 47 ppm (Schlesinger and Vengosh, 2016; and references therein). Due to the contribution of gaseous and particulate B into rivers via precipitation (see atmospheric inputs), this section discusses the contribution of the effluents of coal combustion residuals (CCRs) to rivers. The large variations in the B concentrations and $\delta^{11}B$ values of the leachates of CCRs, which range from 1 to 142 ppm and −19 to +16‰, respectively, are attributed to different coal sources considering that the isotopic fractionation associated with coal combustion and leaching from CCRs is apparently small (Davidson and Bassett, 1993; Ruhl et al., 2014; Williams and Hervig, 2004). Surface water and groundwater under the influence of the leaching of CCRs exhibit $\delta^{11}B$ values (from −9.9 to +30.0‰) that are different from background water values (Harkness et al., 2016). The mean $\delta^{11}B$ value of the leachates of CCRs mentioned above is +0.5 ± 9.8‰ (1SD, n = 54). The $\delta^{11}B$ values of oil- and gas-produced water, which range from +25.5 to +51‰ (average: +33.8 ± 6.8‰, 1SD, n = 52), are quite different from those of the leachates of CCRs (Warner et al., 2014; Warner et al., 2013).

Boron ore products from two major B producers (Turkey and USA) are used for glass (51%), ceramics (13%), agriculture (14%), detergents (3%) and other uses (19%) (Barth, 2000; Kot, 2015). B used in detergents, fertilizers and insecticides probably contributes substantially to rivers. Industrial products are manufactured from borate minerals that are dominantly exploited in non-marine evaporite deposits in Turkey and the USA (Barth, 2000; and references therein). Moreover, industrial manufacturing processes are unlikely to cause significant isotopic fractionation (Barth, 1998; Barth, 2000; Palmer and Helvaci, 1995; Palmer and Helvaci, 1997; Swihart et al., 1996). In China, borate ore deposits exhibit a wide range of $\delta^{11}B$ values from −19.5 to +11.1‰ (Jiang, 2001; Jiang et al., 1997). In general, non-marine borates have low values (Fig. 7a). The $\delta^{11}B$ values of industrial and urban effluents should fall within the same range because all of these products originate from borate minerals. However, the mean $\delta^{11}B$ value of urban wastewater is slightly higher than that of industrial wastewater, probably because of the different sources of urban and industrial wastewater.

Agricultural wastewater mostly refers to fertilizer and animal manure. The variation in the $\delta^{11}B$ values of mineral fertilizer is likely attributed to different mineral sources; for example, the $\delta^{11}B$ values in the USA range from −2 to +0.7‰ (Komor, 1997), and the $\delta^{11}B$ values in France range from −8 to +7‰ (Widory et al., 2005). Moreover, animal manure exhibits remarkably higher $\delta^{11}B$ values (Fig. 7b), which are probably due to variations in the diet and physiology of different animals (Komor, 1997). The combination of B and N isotopes has been used to identify the contamination of groundwater and surface water (Briand et al., 2017; Bronders et al., 2012; Puig et al., 2017; Widory et al., 2004; Widory et al., 2013; Widory et al., 2005). The mean $\delta^{11}B$ values of industrial, urban, and agricultural wastewater are −6.9 ± 7.5‰ (1SD, n = 142), +1.2 ± 5.2‰ (1SD, n = 67), and +12.3 ± 10.7‰ (1SD, n = 45), respectively, and the $\delta^{11}B$ values of these subgroups of wastewater are shown in Fig. 7b.

3. Processes of boron in catchments

Could we regard the B isotopes of rivers as the simple mixture of different sources? If not, what processes influence the B isotopes of rivers, where do the processes occur, and to what extent do those processes change the B isotopes of rivers? Here, we conduct a preliminary investigation of the processes on the continental surface.

3.1. Mixing of sources of B in rivers

The behavior of B and the extent to which it behaves as a conservative element should be evaluated in river systems. We hence assess the behavior of B during adsorption on river sediments, throughout the biological cycle in aquatic ecosystems, and during carbonate precipitation from river water.

Assuming that the suspended particulates (up to 400 mg/L) are illite (i.e., clay minerals with the maximum B adsorption, see Section 2.4.2), at T = 25°C pKa = 9.23 (Baes and Mesmer, 1976), a pH of 8 and high B concentrations of 40 ppb in rivers (Lemarchand et al., 2002b), based on the calculation of Keren and Mezuman (1981), the proportion of B adsorbed on solids is less than 0.5%, which is consistent with previous results (i.e., lower than 1%) (Chetelat et al., 2009b; Lemarchand and Gaillardet, 2006; Rose et al., 2000b). Moreover, in sediments from seawater, which exhibits higher B concentrations relative to rivers and a proper pH (see Section 2.4.2), the proportion of adsorbed B is still approximately 10% (Spivack et al., 1987). Therefore, the adsorption of B does not significantly change the B concentrations and $\delta^{11}B$ values in rivers (Chetelat et al., 2009b; Gaillardet and Lemarchand, 2018; Lemarchand and Gaillardet, 2006; Rose et al., 2000b).

The biological uptake of B by aquatic plants, algae, and animals is usually neglected in river studies. Boron is generally not consumed by microorganisms in river systems (Chetelat and Gaillardet, 2005; Guinoiseau et al., 2018; Widory et al., 2005). However, B plays a key role in plants, where it participates in the cell wall structure and processes such as polyol transport, nitrogen fixation, and reproduction (Blevins and Lukaszewski, 1998; Brown et al., 2002; Roux et al., 2015); thus, ignoring the uptake of B by aquatic plants may underestimate the impact of biological effects in rivers. Furthermore, the role of biological effects on B isotopes in soils remains debatable. A few studies have showed that B isotopic fractionation occurs between plants and soil solutions ($\Delta^{11}B_{plant\text{-}soilwater} = -10 \pm 5‰$) (Cividini et al., 2010) and between plant tissues (i.e., leaves are generally enriched in ^{11}B compared to roots or stems) (Geilert et al., 2015; Sun et al., 2014; Xu et al., 2015), whereas Schmitt et al. (2012) proposed that absorption by plant roots does not cause substantial isotopic fractionation. The biological cycle of boron in aquatic ecosystems is poorly understood.

Many studies have focused on B isotopes during carbonate precipitation in marine environments; however, little is known about the effects of carbonate precipitation on B isotopes in rivers. Carbonate precipitation occurs in a few karstic catchments (e.g., Dominguez-Villar et al., 2017; Li et al., 2010) and in arid areas, such as Northern India (e.g., Bickle et al., 2005). Experiments of calcite or aragonite precipitation (Kaczmarek et al., 2016; Mavromatis et al., 2015; Noireaux et al., 2015; Sanyal et al., 2000; Uchikawa et al., 2015; Xiao et al., 2008) have indicated that the deposition of carbonate will shift the $\delta^{11}B$ values of water; however, it remains unclear how the $\delta^{11}B$ values in rivers will change. A recent study of adsorption on calcite shows a wide range of values of $\Delta^{11}B_{ads\text{-}sol} = -24.5$ to +5.5‰ at 8 < pH < 12 (Saldi et al., 2018). The precipitation of carbonates can increase the $\delta^{11}B$ values of liquids in thermal springs by causing the adsorption of ^{10}B on solids, as observed in Tibet (Yuan et al., 2014). The B contents and isotopes of river water in arid areas, karstic catchments, or rivers with high suspended sediment loads are likely not conservative. However, carbonate precipitation does not often occur in other types of rivers where B and B isotopes can be considered conservative.

Assuming that B is conservative during in situ riverine processes and that B isotopic fractionation mainly occurs in regolith and groundwater, we can establish a combined mixing model of the different sources of B (Chetelat and Gaillardet, 2005; Chetelat et al., 2009b; Gaillardet et al., 1999) with the fractionation derived from related processes in the basin to describe the $\delta^{11}B$ values of river water ($\delta^{11}B_{river}$) (for details, see Supplementary B.2.1):

$$\frac{[B]_{river}}{[Na]_{river}} = \sum \frac{[B]_i + \Delta[B]_j}{[Na]_i} * \alpha(Na)_i \quad (1)$$

$$\delta^{11}B_{river} * \frac{[B]_{river}}{[Na]_{river}} = \sum \delta^{11}B_i * \frac{[B]_i}{[Na]_i} * \alpha(Na)_i + \sum \Delta^{11}B_j * \frac{\Delta[B]_j}{[Na]_i} * \alpha(Na)_i \quad (2)$$

where $\alpha(Na)_i$ represents the mixing proportion of Na from different sources (i = atmosphere, evaporite, granite, basalt, shale, and anthropogenic inputs); $[B]_{river}$ and $[Na]_{river}$ are the concentrations of B and Na of river water, respectively; $[B]_i$ and $\delta^{11}B_i$ are the B concentration and the $\delta^{11}B$ value of the reservoir i, respectively. During release of B from the reservoir i to rivers, the processes j would change the B of the reservoir i (j = dissolution, precipitation, and biological cycling in regolith). The B concentration and $\delta^{11}B$ value of the portion of changed B are the difference in B concentration ($\Delta[B]_j$) and $\delta^{11}B$ value ($\Delta^{11}B_j$) between the reservoir i and the input to rivers, respectively. [Cl]/[B] ratios can also be substituted for [Na]/[B] ratios (Lemarchand and Gaillardet, 2006). The inventory of the reservoirs of B isotopes (Section 2) can be applied in mixing equation (2) for river water only on a large scale (mainly continental scale) due to the wide range of B reservoirs. In other words, the large uncertainties of the reservoirs of B isotopes probably reflect that B is highly mobile; hence, when B isotopes are studied in a small catchment, the local geology and lithology should be investigated to determine the appropriate end-member of B.

3.2. B isotopic fractionation during water-rock interactions and biological cycling

Water-rock interactions on the continental surface can lead to considerable variability in the dissolved $\delta^{11}B$ values of rivers (Chetelat et al., 2009b; Lemarchand and Gaillardet, 2006; Rose et al., 2000b). In groundwater and regolith, boron in solution can be significantly adsorbed on the surfaces of secondary minerals and organic matter or be coprecipitated into secondary minerals (Gaillardet and Lemarchand, 2018). Several studies have suggested that B isotopic fractionation depends on the temperature, pH, mineralogy, water-rock ratio, and organic matter during water-rock interactions on the continental surface (Deyhle and Kopf, 2005; Lemarchand et al., 2005; Lemarchand et al., 2007; Palmer et al., 1987; Palmer and Swihart, 1996; Saldi et al., 2018; Voinot et al., 2013; Williams et al., 2001a; Xiao and Wang, 2001). The biological cycle may not considerably influence the boron in river water during in situ riverine processes, but it can largely affect the B isotopic composition of soil solutions in regolith, such as in the Strengbach catchment (Cividini et al., 2010; Lemarchand et al., 2012). Thus, we focus on the water-rock interactions and biological cycle of B in groundwater and regolith.

3.2.1. Models of B isotopic fractionation controlled by adsorption/desorption in groundwater

Although the adsorption of B on river sediments may not dominate the B isotopic fractionation during in situ riverine processes, the adsorption/desorption in groundwater can largely affect the boron of river water through baseflow. After boron is released from primary minerals, it is adsorbed on mineral surfaces or coprecipitated into minerals. The equations describing the exchange of B between solution and mineral surfaces can be written as (Gaillardet and Lemarchand, 2018; Lemarchand and Gaillardet, 2006; Lemarchand et al., 2015):

$$[B]_{sol} = \frac{W_R}{W_R + Kd} * [B]_T \quad (3)$$

$$R_{sol} = \frac{Kd + W_R}{\alpha * Kd + W_R} * R_T \quad (4)$$

where $[B]_{sol}$ and $[B]_T$ are the concentrations of B dissolved in solution at equilibrium and the total quantity of B (adsorbed and dissolved) per mass of water, respectively; W_R is the water/rock ratio; Kd is the partition coefficient of B ($Kd = [B]_{ads}/[B]_{sol}$); R_{sol} and R_T are the $^{11}B/^{10}B$ ratios of the solution at equilibrium and the total $^{11}B/^{10}B$ ratios, respectively; and α is the fractionation factor between the solids and solution ($\alpha = R_{ads}/R_{sol}$) (for details, see Supplementary B.2.2).

In the Mackenzie basin (mainly composed of shale), the adsorption model was applied to describe the rapid ion exchange reactions in groundwater; furthermore, a reactive transport model reveals that the $\delta^{11}B$ value of river water is sensitive to hydrological conditions, weathering rates, the residence time of groundwater, and the host rock exchange properties (Lemarchand and Gaillardet, 2006). In the Susquehanna Shale Hills, B is primarily removed by the erosion of fine particles (clay) from regolith rather than chemical weathering (Noireaux et al., 2014; Sullivan et al., 2016), implying that a basin mainly composed of shale may be dominated by adsorption in groundwater due to the low weathering rate of shale.

3.2.2. Models of B isotopic fractionation controlled by weathering in regolith

The steady-state mass balance model established by Bouchez et al. (2013) can be used to describe the stable isotopic compositions (e.g., Li, B, Ca, and Si) of soil solution during the weathering of silicate rocks in regolith. This model can also be applied in Eq. (2) as $\Delta^{11}B_j$ and $\Delta[B]_j$ to predict how the $\delta^{11}B$ of river water would vary in response to the weathering of regolith on a catchment or continental scale when the B of river water primarily originates from the weathering of regolith. The following assumptions in the model will be revisited to confirm that they are suitable for B isotopes. Based on the characteristics of B discussed above, it is reasonable to assume that the precipitation of secondary minerals and biological uptake result in B isotopic fractionation in regolith (Bouchez et al., 2013). In addition to the dissolution of

Table 1
Symbols in models.

Symbols	Definition
$\delta^{11}B_{rock}$	B isotopic composition of bedrock
$\delta^{11}B_{diss}$	B isotopic composition of soil- or river water
$\Delta^{11}B_{prec}$	B isotopic fractionation factor associated with the precipitation of secondary weathering products (including adsorption) (between secondary products and soil water)
$\Delta^{11}B_{upt}$	B isotopic fractionation factor associated with uptake by plants (between plants and soil water)
S_{rock}	Flux of dissolution of B ("solubilization") from primary minerals at the weathering front
S_{prim}	Flux of dissolution of B ("solubilization") from primary minerals in the regolith
E_{sec}	Flux of erosion of B contained in secondary weathering products
E_{org}	Flux of erosion of B contained in organic matter
$[B]_{rock}$	Concentration of B in bulk rock
$[B]_{prim}$	Concentration of primary mineral-bound B in the regolith
$[B]_{sec}$	Concentration of secondary weathering product-bound B in the regolith
$[B]_{org}$	Concentration of organic matter-bound B in the regolith

Adapted from Bouchez et al. (2013).

biotite causing B isotopic fractionation (Voinot et al., 2013), the incongruent weathering of primary rock-forming minerals can also lead to B isotopic fractionation due to the different dissolution rates and different $\delta^{11}B$ values of primary minerals (Kaliwoda et al., 2011; MacGregor et al., 2013; Zhao et al., 2015). Nevertheless, considering the assumption that regolith is treated as a "batch reactor" and exits at steady-state, we can assume that no B isotopic fractionation occurs during the dissolution of primary minerals and desorption of secondary minerals (Bouchez et al., 2013). Although Rayleigh fractionation has been used to interpret B isotopic data in the weathering zone (e.g., Rudnick et al., 2004; Thompson et al., 2007; Tipper et al., 2012), the B data of these profiles do not fit this model (Lemarchand et al., 2012; Sullivan et al., 2016). Rather, the model envisions the entire regolith as a "batch reactor"; thus, it is not suitable to use Rayleigh effects in this case (see discussion in Bouchez et al. (2013)). After confirmation of these assumptions, the model is applied to describe the $\delta^{11}B$ value of soil water ($\delta^{11}B_{diss}$) in regolith, which is expressed as (see Table 1 for symbols):

$$\delta^{11}B_{diss} = \delta^{11}B_{rock} - \frac{\Delta^{11}B_{prec}{}^{*}E_{sec} + \Delta^{11}B_{upt}{}^{*}E_{org}}{S_{rock} + S_{prim}} \quad (5)$$

Eq. (5) illustrates that $\delta^{11}B_{diss}$ is dependent on lithology ($\delta^{11}B_{rock}$), fractionation factors ($\Delta^{11}B_{prec}$ and $\Delta^{11}B_{upt}$), and the fluxes of erosion (E_{sec}, and E_{org}) and weathering (S_{rock} and S_{prim}) in regolith. The $\delta^{11}B_{rock}$ values of different types of silicate rocks are discussed in Section 2.4.1; however, the combined effects of fractionation and the fluxes of weathering and erosion on $\delta^{11}B_{diss}$ have not yet been fully recognized. To apply this model, it is essential to elucidate the B isotopic fractionation during weathering processes. The B isotopic fractionation during dissolution, precipitation, and uptake are discussed below.

Very limited information is available concerning the B isotopic fractionation during the dissolution of primary minerals. In biotite, large differences in the $\delta^{11}B$ values of different crystallographic sites have been reported (Voinot et al., 2013). Likewise, illite and smectite exhibit similar $\delta^{11}B$ patterns ($\delta^{11}B_{interlayer\text{-}site} > \delta^{11}B_{tetrahedral\text{-}site}$) (Williams and Hervig, 2002; Williams et al., 2001a), and these can be extrapolated to other phyllosilicates (Voinot et al., 2013). Thus, the B isotopic fractionation during the dissolution of phyllosilicates can be attributed to the different dissolution rates and different $\delta^{11}B$ values of the interlayer and structural sites (Voinot et al., 2013). Nonetheless, as for the regolith, we surmise that the incongruent weathering of rock-forming minerals is a more general scenario relative to the dissolution of phyllosilicates. The $\delta^{11}B$ values of primary minerals and B isotopic fractionation during the dissolution of primary rock-forming minerals both warrant further study.

Generally, the precipitation of secondary minerals comprises the adsorption of $B(OH)_4^-$ on mineral surfaces and its later substitution for Si or Al in tetrahedral sites, which are both preferentially enriched in ^{10}B (Muttik et al., 2011; Palmer et al., 1987; Palmer and Swihart, 1996; Williams et al., 2001a). During adsorption, $\Delta^{11}B_{clay\text{-}solution}$ is pH-dependent at low temperatures and ranges from $-32 \pm 3‰$ to $-25 \pm 2‰$ at pH values ranging from 6.8 to 7.8 (Palmer et al., 1987; Spivack et al., 1987). Likewise, $\Delta^{11}B_{oxy\text{-}solution}$ is pH-dependent; in particular, $\Delta^{11}B_{goethite\text{-}solution} = -40‰$ at pH < 8 and $\Delta^{11}B_{birnessite\text{-}solution} = -15‰$ at pH < 8.5 (Lemarchand et al., 2007). Additionally, B isotopic fractionation during B adsorption onto host minerals in aquifer shows pH-dependency (Lemarchand et al., 2015). During substitution in the structural sites of minerals, B isotopic fractionation depends primarily on temperature, pH, and salinity (Boschi et al., 2008; Muttik et al., 2011; Pennisi et al., 2009; Vils et al., 2009). Furthermore, Liu and Tossell (2005) indicated that further fractionation during the substitution of structural B (noted as $\Delta^{11}B_{substitution}$) occurs between B $(OH)_4^-$(aq) and tetrahedral B in phyllosilicates.

The B isotopic fractionation factor of uptake by plants ($\Delta^{11}B_{upt}$) from soil water, which ranges from −10 to −5‰, indicates that ^{10}B is slightly enriched in plants (Cividini et al., 2010), which is consistent with the preferential incorporation of ^{10}B into organic matter ($\Delta^{11}B_{humic\ acid\text{-}sol} = -25‰$) (Lemarchand et al., 2005). Moreover, only a few studies have reported B isotopic fractionation between plant tissues, for instance, fractionation between plant tissues ($\Delta^{11}B_{leaves\text{-}roots} = +27‰$ in bell pepper) (Geilert et al., 2015) and fractionation between hydro-soluble and structural B ($\Delta^{11}B_{sap\text{-}cell\ wall} = -15$ to $+4.6‰$) (Sun et al., 2018). A few studies have indicated that the B in plants can be transferred as boric acid during its uptake and transport and that it can be fixed in the cell wall as borate (Blevins and Lukaszewski, 1998; Geilert et al., 2015; Reid, 2014). However, little is known about the influence of plant physiology and the mineralization of organic matter on B isotopes in the biological cycle. Thus, the B isotopic fractionation during biological cycling may present large variability.

For this model, we assume that $\Delta^{11}B_{prec}$ is equal to the B isotopic fractionation during adsorption ($\Delta^{11}B_{ads}$) because $\Delta^{11}B_{prec}$ mainly results from adsorption. The relationship between $\Delta^{11}B_{ads}$ and pH has been verified to be linear in a narrow range of pH values (6.8–8) (Palmer et al., 1987); otherwise, it is a sigmoidal curve (Lemarchand et al., 2005; Lemarchand et al., 2007). Nevertheless, to make a first order estimation of $\Delta^{11}B_{prec}$, we tentatively assume that $\Delta^{11}B_{prec}$ is linearly related to the pH of the solution and ranges from −32 to 0‰ (pH from 5.5 to 9) (details see Supplementary B.3), based on a summary of B isotopic fractionation during adsorption (Gaillardet and Lemarchand, 2018). In contrast, $\Delta^{11}B_{upt}$ is mainly dependent on the plant physiology rather than the weathering conditions in regolith. Thus, we assume that $\Delta^{11}B_{upt}$ remains constant under different degrees of weathering of regolith.

It is difficult to directly determine the fluxes of B in the different compartments of regolith, which hinders the application of this model. To overcome this problem, we convert the B flux into a function of a parameter that is indicative of weathering conditions using the same method as Bouchez et al. (2013). For the derivation of the model, see Supplementary B.3. Eq. (5) is converted to a function of the chemical depletion fraction, and the $\delta^{11}B$ value of soil water can be written as follows:

$$\delta^{11}B_{diss} - \delta^{11}B_{rock} = \frac{\frac{[B]_{sec}}{[B]_{rock}}\Delta^{11}B_{prec} + \frac{[B]_{org}}{[B]_{rock}}\Delta^{11}B_{upt}}{\frac{[B]_{prim}}{[B]_{rock}} - \frac{1}{1-CDF}} \quad (6)$$

The chemical depletion fraction (CDF) is defined as $CDF = 1\text{-}[X_i]_{rock}/[X_i]_{regolith} = W/D$, where $[X_i]_{regolith}$ and $[X_i]_{rock}$ are the concentrations of immobile element in regolith and parent rock, respectively; and W and D represent the chemical weathering rate and the total denudation rate, respectively (Riebe et al., 2003; Riebe et al., 2001). The CDF is used as a proxy of the chemical weathering intensity (Dellinger et al., 2015; Dixon et al., 2009; Riebe et al., 2003). We assume that the CDF values increase with decreasing pH; hence, $\Delta^{11}B_{prec}$ increases with increasing CDF values. The values of CDF normally vary between 0 and 0.5 in granitic lithologies (Riebe et al., 2004; Schoonejans et al., 2016). We use the model of Ferrier and Kirchner (2008) to calculate the concentrations of minerals (quartz, plagioclase, K-feldspar, biotite, kaolinite) in a regolith developed on granite at steady-state conditions, the non-dimensional denudation rate ($D_{non\text{-}dimensional}$), the non-dimensional weathering rate ($W_{non\text{-}dimensional}$), and the CDF (calculated by $W_{non\text{-}dimensional}/D_{non\text{-}dimensional}$) (Fig. 8a). Considering that B contents generally decrease in the order of muscovite > plagioclase > biotite > K-feldspar > quartz (Leeman and Sisson, 1996) and based on their proportions in granites, we assume that B is hosted only by plagioclase and biotite in unweathered granite and in equal proportions. Likewise, we assume that kaolinite is the only host of B as a secondary product. Thus, the concentrations of minerals are only shown in Fig. 8a for plagioclase, biotite and kaolinite. We assume that the B contents of unweathered rock, secondary minerals, and organic

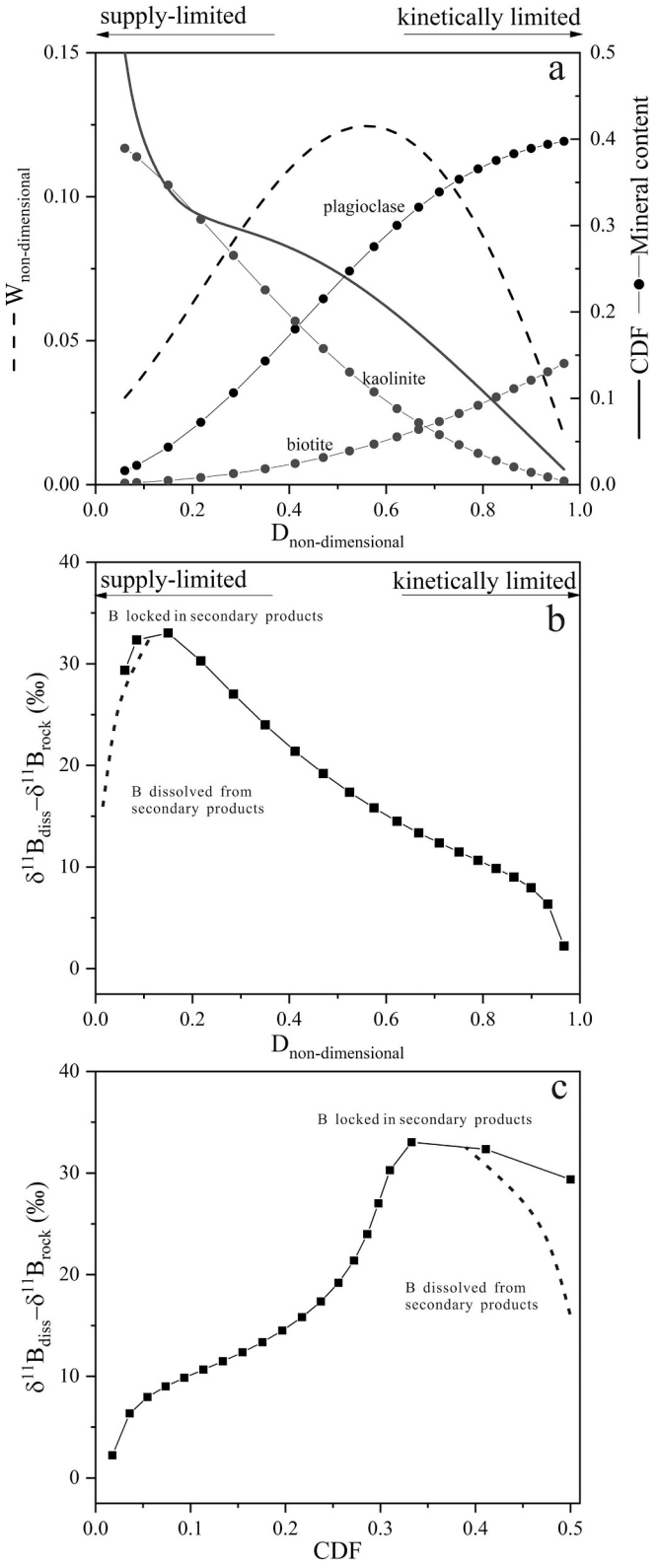

Fig. 8. Model of $\delta^{11}B$ of soil water in weathering of regolith following the results of Ferrier and Kirchner (2008) and Bouchez et al. (2013). (a) The steady-state concentrations of minerals (plagioclase, biotite, and kaolinite) in regolith developed on granite, non-dimensional denudation rate ($D_{non\text{-}dimensional}$), non-dimensional weathering rate ($W_{non\text{-}dimensional}$), and CDF. (b) Changes in $\delta^{11}B_{diss}-\delta^{11}B_{rock}$ with $D_{non\text{-}dimensional}$ in two types of weathering regimes. (c) Variations in $\delta^{11}B_{diss}-\delta^{11}B_{rock}$ with CDF. The dashed lines in Fig. 8b and c reflect rough estimates of the expected trend of decrease in $\delta^{11}B_{diss}-\delta^{11}B_{rock}$ when B is dissolved from secondary minerals.

matter are 10 ppm, 38.7 ppm, and 100 ppm, respectively; $\Delta^{11}B_{prec}$ ranges from −32 to 0‰, increasing linearly, and $\Delta^{11}B_{upt}$ is −10‰ (for details; see Supplementary B.3).

The influences of climatic and tectonic forcing on chemical weathering on the catchment or continental scale have been extensively studied (Dixon et al., 2012; Ferrier et al., 2012; Godderis et al., 2017; Maher and Chamberlain, 2014; Riebe et al., 2017; Riebe et al., 2001; West et al., 2005). To investigate how the $\delta^{11}B$ of river water will change in response to these two types of forcing, two types of weathering regimes are considered: (1) a supply-limited regime is characterized by a low denudation rate (D), high weathering intensity (CDF = W/D), and long regolith residence time, which means that primary minerals are nearly completely altered before their erosion and that many secondary minerals are formed, thus implying tectonic controls on chemical weathering rates; and (2) a kinetically limited regime is characterized by a high D, low CDF, and short regolith residence time, which means that primary minerals are incompletely altered before being eroded away and that fewer secondary minerals are formed, thus implying climatic controls on chemical weathering rates (Dixon et al., 2012; Ferrier et al., 2016; Riebe et al., 2017; Riebe et al., 2004; West et al., 2005). The variations in $\delta^{11}B_{diss}-\delta^{11}B_{rock}$ in the two types of weathering regimes with $D_{non\text{-}dimensional}$ and CDF are shown in Fig. 8b and c, respectively. In the supply-limited regime, the precipitation of secondary minerals controls the variations in the $\delta^{11}B_{diss}$ in regolith, e.g., the Strengbach catchment (Cividini et al., 2010), leading to an increase in $\delta^{11}B_{diss}-\delta^{11}B_{rock}$ with lower $D_{non\text{-}dimensional}$, whereas secondary minerals could also dissolve and release isotopically light B that was adsorbed earlier, i.e., when the regolith had very low $D_{non\text{-}dimensional}$ (< 0.15) values, thus leading to a decrease in $\delta^{11}B_{diss}-\delta^{11}B_{rock}$ with lower $D_{non\text{-}dimensional}$. In the kinetically limited regime, biological cycling should control the variations in the $\delta^{11}B_{diss}$ in regolith, e.g., the Mule Hole CZO (Gaillardet and Lemarchand, 2018), thus causing $\delta^{11}B_{diss}$ to become closer to $\delta^{11}B_{rock}$ with higher denudation rates because a high denudation rate may cause less vegetation or make less B available for plants and lead to the formation of fewer secondary minerals. The relationship between the denudation rate (or CDF) and $\delta^{11}B_{diss}-\delta^{11}B_{rock}$ is not monotonous due to the dissolution of secondary minerals, which is similar to the processes of Li isotopes (Dellinger et al., 2015). This indicates that additional constraints are required to distinguish between the two regimes. Based on the role of fluxes of erosion in Eq. (5), B isotope geochemistry of suspended sediments could serve as an additional constraint on understanding continental weathering. In addition to precipitation and biological cycling, the lithology can also affect $\delta^{11}B_{diss}$ through the $\delta^{11}B$ value of the bedrock and the incongruent weathering of rock-forming minerals. The influence of dissolution of primary minerals and of precipitation of secondary minerals on the $\delta^{11}B_{diss}$ values also depends on the hydrological conditions (Gaillardet and Lemarchand, 2018).

The results (Fig. 8b and c) are based on the assumptions of $\Delta^{11}B_{prec}$, $[B]_{org}/[B]_{rock}$, and $[B]_{sec}/[B]_{rock}$, but limited information is available about how they respond to changes in the CDF, which can cause great uncertainties. To evaluate the impacts of different parameters, we performed a simple sensitivity analysis (Fig. 9). Different values are assigned to $\Delta^{11}B_{prec}$, $\Delta^{11}B_{upt}$, $[B]_{prim}/[B]_{rock}$, $[B]_{org}/[B]_{rock}$, and $[B]_{sec}/[B]_{rock}$ (for details, see Supplementary B.3). The changes in $\Delta^{11}B_{prec}$ and $[B]_{sec}/[B]_{rock}$ significantly decrease $\delta^{11}B_{diss}-\delta^{11}B_{rock}$ in the supply-limited regime (high CDF) but only slightly change $\delta^{11}B_{diss}-\delta^{11}B_{rock}$ in the kinetically limited regime (low CDF) (Fig. 9a). Changing $\Delta^{11}B_{upt}$ to −15‰ slightly increased $\delta^{11}B_{diss}-\delta^{11}B_{rock}$, while changing $\Delta^{11}B_{upt}$ to +10‰ remarkably changed $\delta^{11}B_{diss}-\delta^{11}B_{rock}$ at a low CDF, which resulted in an initial decrease and later increase (Fig. 9b). Similarly, changing $[B]_{org}/[B]_{rock}$ will slightly change $\delta^{11}B_{diss}-\delta^{11}B_{rock}$ at a high CDF, whereas increasing $[B]_{org}/[B]_{rock}$ at a low CDF will cause an opposite trend that first decreases and then increases (Fig. 9c). The effects of $\Delta^{11}B_{upt}$ and $[B]_{org}/[B]_{rock}$ indicate that biological cycling dominates the B isotopic fractionation in a kinetically limited regime. Decreasing

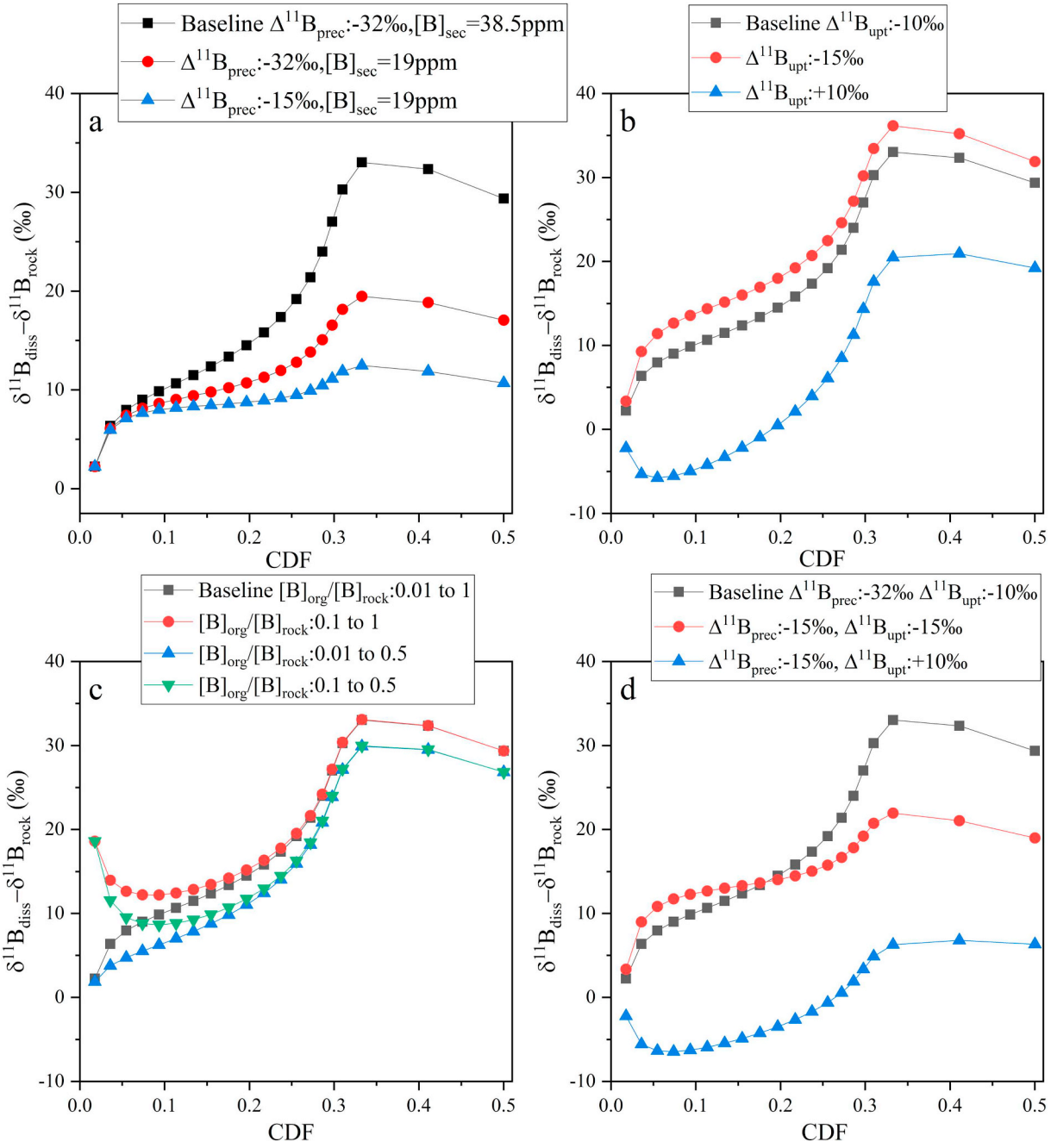

Fig. 9. Sensitivity analysis of parameters in the model. The baseline is used for the same parameters in Fig. 8b and c. For $[B]_{prim}/[B]_{rock}$, $[B]_{sec}/[B]_{rock}$, $[B]_{org}/[B]_{rock}$, $\Delta^{11}B_{prec}$, and $\Delta^{11}B_{upt}$, see Supplementary B.3. (a) $\delta^{11}B_{diss}-\delta^{11}B_{rock}$ responds to changes in $\Delta^{11}B_{prec}$ and $[B]_{sec}/[B]_{rock}$. (b) Different trends of $\delta^{11}B_{diss}-\delta^{11}B_{rock}$ in response to changes in $\Delta^{11}B_{upt}$. (c) Different trends of $\delta^{11}B_{diss}-\delta^{11}B_{rock}$ in response to changes in $[B]_{org}/[B]_{rock}$. (d) Responses of $\delta^{11}B_{diss}-\delta^{11}B_{rock}$ to changes in $\Delta^{11}B_{prec}$ and $\Delta^{11}B_{upt}$.

$\Delta^{11}B_{prec}$ to −15‰ and increasing $\Delta^{11}B_{upt}$ to −15‰ led to minor changes in $\delta^{11}B_{diss}-\delta^{11}B_{rock}$ at a moderate CDF (0.1–0.3). Using a $\Delta^{11}B_{prec}$ value of −15‰ and a $\Delta^{11}B_{upt}$ value of +10‰ led to significantly low values of $\delta^{11}B_{diss}-\delta^{11}B_{rock}$. Variations in both $\Delta^{11}B_{prec}$ and $\Delta^{11}B_{upt}$ will significantly change the trends of $\delta^{11}B_{diss}-\delta^{11}B_{rock}$ (Fig. 9d), suggesting that the trends of $\delta^{11}B_{diss}-\delta^{11}B_{rock}$ are sensitive to B isotopic fractionation during the precipitation of secondary minerals and biological cycling. However, thus far, the values of $\Delta^{11}B_{prec}$ and $\Delta^{11}B_{upt}$ have mostly been determined by experiments, suggesting that better understanding the behavior of B isotopes in regolith requires extensive field studies.

4. Conclusions

We evaluate the B reservoirs of meteoric precipitation, evaporites, carbonates, silicate rocks, and anthropogenic inputs to investigate the provenance constraints on B isotopes in river water on a continental scale. Based on the source and evolution of boron reservoirs, the following inventories are estimated using subgroups of each reservoir to fit most types of basins. (1) Atmospheric inputs: mixing and Rayleigh effects are mainly responsible for the variations in the $\delta^{11}B$ values of meteoric precipitation, which result in marine ($\delta^{11}B$ = +37 ± 7‰, Cl/B = 455 ± 376), anthropogenic ($\delta^{11}B$ = +9 ± 10‰, Cl/

B = 98 ± 164), and mixing types ($\delta^{11}B$ = +17 ± 13‰, Cl/B = 148 ± 122) of meteoric precipitation. (2) Carbonates: the B contributions of carbonate dissolution to rivers are negligible because continental carbonates have low B contents and marine carbonates lose B after diagenesis. (3) Evaporites: marine and non-marine evaporites have distinct $\delta^{11}B$ values, primarily reflecting their different depositional environments. Marine evaporites have a $\delta^{11}B$ value of +27 ± 9.4‰ and a Cl/B value of 1300, whereas non-marine evaporites have a $\delta^{11}B$ value of −2 ± 8.6‰ and a Cl/B value of 250 ± 360. (4) Silicate rocks: igneous rocks (excluding tourmaline-bearing rocks) have a mean B content of 11.6 ± 13.4 ppm. S-type granites that are tourmaline-free have an estimated $\delta^{11}B$ value of −14.2 ± 4.9‰, B content of 62.5 ± 12.5 ppm, and Na/B value of 140 ± 34. Non-S-type granites have a $\delta^{11}B$ value of −8.9 ± 6.7‰, B content of 11 ± 10 ppm, and Na/B value of 1190 ± 170. Intraplate basalts exhibit a $\delta^{11}B$ value of −5.2 ± 4.4‰ and a Na/B value of 3300 ± 770. Subduction-related basalts have a $\delta^{11}B$ value of +0.3 ± 7.3‰ and a Na/B value of 1060 ± 830. Shale has high B contents of siliciclastic sedimentary rocks (B content = 104 ± 92 ppm and $\delta^{11}B$ = −12 ± 0.5‰). The inferred $\delta^{11}B$ values of marine and continental shales are −8‰ and −16‰, respectively. The effects of metamorphism can vary widely depending on the geologic setting and types of protolith. (5) Anthropogenic inputs: the $\delta^{11}B$ values of the leachates of coal combustion residuals, oil and gas-produced water, and industrial, urban, and agricultural wastewater are assumed to be +0.5 ± 9.8‰, +33.8 ± 6.8‰, −6.9 ± 7.5‰, +1.2 ± 5.2‰, and +12.3 ± 10.7‰, respectively. The variability in the $\delta^{11}B$ values of contamination are probably due to their different sources. It is important to highlight that the preliminary estimates of B reservoirs suffer from large uncertainties; however, this inventory of B isotopes can be useful for understanding the mixing of end-members in rivers on a continental scale. In contrast, rivers on a catchment scale require extensive work to determine the end-members of B based on their local lithological and geological conditions.

The water-rock interactions and the biological cycle of B are the principal processes leading to B isotopic fractionation in regolith and groundwater, whereas adsorption on sediments leads to minor B isotopic fractionation in rivers. In groundwater, rapid ion exchange reactions can be described by the adsorption model, and the reactive transport model reveals that the $\delta^{11}B$ values of river water are sensitive to hydrological conditions. In regolith, the steady-state mass balance model is used to predict the B isotope behavior of soil solution during weathering processes and biological cycling. In the supply-limited regime (where chemical weathering is limited by tectonic forcing), the precipitation of secondary minerals controls the variation in the $\delta^{11}B$ values of soil solution ($\delta^{11}B_{diss}$), leading to an increase in $\delta^{11}B_{diss} - \delta^{11}B_{rock}$ with lower denudation rates, whereas $\delta^{11}B_{diss} - \delta^{11}B_{rock}$ will decrease with lower denudation rates when secondary minerals dissolve. In the kinetically limited regime (where chemical weathering is limited by climate), biological cycling controls the variations in the $\delta^{11}B_{diss}$ values in regolith, and $\delta^{11}B_{diss}$ generally becomes closer to $\delta^{11}B_{rock}$ with higher denudation rates. The relationship between the denudation rate (or CDF) and $\delta^{11}B_{diss} - \delta^{11}B_{rock}$ is thus not monotonous, indicating that additional constraints are required to distinguish between the two regimes. These models are preliminary and are affected by considerable uncertainties, but they reveal that the hydrological conditions (in groundwater/soil solution), weathering processes (in regolith/groundwater), and biological cycling (in regolith) can have significant influences on the $\delta^{11}B$ values of river water.

B isotope biogeochemistry of rivers has yet to be fully understood. Future studies need to be done in three regards: constraints on the estimates of B end-members, clarification of the B isotopic fractionation caused by weathering and biological cycling in regolith, and assessment of the atmospheric and biological sub-cycle.

Acknowledgements

We greatly thank four anonymous reviewers for their insightful and constructive comments that significantly improved the manuscript and Dr. Joan-Albert Sanchez-Cabeza for professional editing. This manuscript has benefited from the discussion with Benjamin Chetelat (Tianjin University) and Jun Xiao (Chinese Academy of Sciences). This work was jointly supported by the National Natural Science Foundation of China (Grant No. 41661144042; 41210004).

Appendix A. Supplementary data

Supplementary data to this article can be found online at https://doi.org/10.1016/j.earscirev.2019.01.016.

References

Aggarwal, J., Bohm, F., Foster, G., Halas, S., Honisch, B., Jiang, S.-Y., Kosler, J., Liba, A., Rodushkin, I., Sheehan, T., Jiun-San Shen, J., Tonarini, S., Xie, Q., You, C.-F., Zhao, Z.-Q., Zuleger, E., 2009. How well do non-traditional stable isotope results compare between different laboratories: results from the interlaboratory comparison of boron isotope measurements. J. Anal. At. Spectrom. 24 (6), 825–831. https://doi.org/10.1039/B815240C.

Amiotte-Suchet, P., Probst, J.L., Ludwig, W., 2003. Worldwide distribution of continental rock lithology: implications for the atmospheric/soil CO_2 uptake by continental weathering and alkalinity river transport to the oceans. Glob. Biogeochem. Cycles 17 (2), 1038. https://doi.org/10.1029/2002GB001891.

Anagnostou, E., John, E.H., Edgar, K.M., Foster, G.L., Ridgwell, A., Inglis, G.N., Pancost, R.D., Lunt, D.J., Pearson, P.N., 2016. Changing atmospheric CO_2 concentration was the primary driver of early Cenozoic climate. Nature 533 (7603), 380–384. https://doi.org/10.1038/nature17423.

Anderson, D.L., Kitto, M.E., Mccarthy, L., Zoller, W.H., 1994. Sources and atmospheric distribution of particulate and gas-phase boron. Atmos. Environ. 28 (8), 1401–1410. https://doi.org/10.1016/1352-2310(94)90203-8.

Anovitz, L.M., Grew, E.S., 1996. Mineralogy, petrology and geochemistry of boron: an introduction. In: Crew, E.S., Anovitz, L.M. (Eds.), Boron: Mineralogy, Petrology and Geochemistry. Mineral. Soc. Am.pp. 1–40.

Baes, C.F., Mesmer, R.E., 1976. Hydrolysis of Cations. Wiley, New York.

Barth, S., 1993. Boron isotope variations in nature: a synthesis. Geol. Rundsch. 82 (4), 640–651. https://doi.org/10.1007/BF00191491.

Barth, S., 1998. Application of boron isotopes for tracing sources of anthropogenic contamination in groundwater. Water Res. 32 (3), 685–690. https://doi.org/10.1016/S0043-1354(97)00251-0.

Barth, S.R., 2000. Boron isotopic compositions of near-surface fluids: a tracer for identification of natural and anthropogenic contaminant sources. Water Air Soil Pollut. 124 (1-2), 49–60. https://doi.org/10.1023/a:1005210226830.

Bassett, R.L., 1990. A critical evaluation of the available measurements for the stable isotopes of boron. Appl. Geochem. 5 (5-6), 541–554. https://doi.org/10.1016/0883-2927(90)90054-9.

Bebout, G.E., 2007. Metamorphic chemical geodynamics of subduction zones. Earth Planet. Sci. Lett. 260 (3–4), 373–393. https://doi.org/10.1016/j.epsl.2007.05.050.

Bebout, G.E., Nakamura, E., 2003. Record in metamorphic tourmalines of subduction-zone devolatilization and boron cycling. Geology 31 (5), 407–410. https://doi.org/10.1130/0091-7613(2003)031<0407:rimtos>2.0.co;2.

Benton, L.D., Ryan, J.G., Tera, F., 2001. Boron isotope systematics of slab fluids as inferred from a serpentine seamount, Mariana forearc. Earth Planet. Sci. Lett. 187 (3–4), 273–282. https://doi.org/10.1016/S0012-821X(01)00286-2.

Bickle, M.J., Chapman, H.J., Bunbury, J., Harris, N.B.W., Fairchild, I.J., Ahmad, T., Pomiès, C., 2005. Relative contributions of silicate and carbonate rocks to riverine Sr fluxes in the headwaters of the Ganges. Geochim. Cosmochim. Acta 69 (9), 2221–2240. https://doi.org/10.1016/j.gca.2004.11.019.

Blevins, D.G., Lukaszewski, K.M., 1998. Boron in plant structure and function. Annu. Rev. Plant Physiol. Plant Mol. Biol. 49, 481–500. https://doi.org/10.1146/annurev.arplant.49.1.481.

Boggs, S., 2011. Principles of Sedimentology and Stratigraphy. Pearson Prentice Hall, Boston, pp. 1–560.

Boschi, C., Dini, A., Fruh-Green, G.L., Kelley, D.S., 2008. Isotopic and element exchange during serpentinization and metasomatism at the Atlantis Massif (MAR 30°N): insights from B and Sr isotope data. Geochim. Cosmochim. Acta 72 (7), 1801–1823. https://doi.org/10.1016/j.gca.2008.01.013.

Boschi, C., Bonatti, E., Ligi, M., Brunelli, D., Cipriani, A., Dallai, L., D'Orazio, M., Früh-Green, G.L., Tonarini, S., Barnes, J.D., Bedini, R.M., 2013. Serpentinization of mantle peridotites along an uplifted lithospheric section, Mid Atlantic Ridge at 11° N. Lithos 178, 3–23. https://doi.org/10.1016/j.lithos.2013.06.003.

Bouchez, J., Von Blanckenburg, F., Schuessler, J.A., 2013. Modeling novel stable isotope ratios in the weathering zone. Am. J. Sci. 313 (4), 267–308. https://doi.org/10.2475/04.2013.01.

Briand, C., Sebilo, M., Louvat, P., Chesnot, T., Vaury, V., Schneider, M., Plagnes, V., 2017. Legacy of contaminant N sources to the NO_3^- signature in rivers: a combined isotopic ($\delta^{15}N$-NO_3^-, $\delta^{18}O$-NO_3^-, $\delta^{11}B$) and microbiological investigation. Sci. Rep. 7, 41703.

https://doi.org/10.1038/srep41703.
Bronders, J., Tirez, K., Desmet, N., Widory, D., Petelet-Giraud, E., Bregnot, A., Boeckx, P., 2012. Use of compound-specific nitrogen ($\delta^{15}N$), oxygen ($\delta^{18}O$), and bulk boron ($\delta^{11}B$) isotope ratios to identify sources of nitrate-contaminated waters: a guideline to identify polluters. Environ. Forensic 13 (1), 32–38. https://doi.org/10.1080/15275922.2011.643338.
Brounce, M., Feineman, M., LaFemina, P., Gurenko, A., 2012. Insights into crustal assimilation by Icelandic basalts from boron isotopes in melt inclusions from the 1783-1784 Lakagigar eruption. Geochim. Cosmochim. Acta 94, 164–180. https://doi.org/10.1016/j.gca.2012.07.002.
Brown, P.H., Bellaloui, N., Wimmer, M.A., Bassil, E.S., Ruiz, J., Hu, H., Pfeffer, H., Dannel, F., Romheld, V., 2002. Boron in plant biology. Plant Biol. 4 (2), 205–223. https://doi.org/10.1055/s-2002-25740.
Calabrese, S., Aiuppa, A., Allard, P., Bagnato, E., Bellomo, S., Brusca, L., D'Alessandro, W., Parello, F., 2011. Atmospheric sources and sinks of volcanogenic elements in a basaltic volcano (Etna, Italy). Geochim. Cosmochim. Acta 75 (23), 7401–7425. https://doi.org/10.1016/j.gca.2011.09.040.
Carrano, C.J., Schellenberg, S., Amin, S.A., Green, D.H., Kupper, F.C., 2009. Boron and marine life: a new look at an enigmatic bioelement. Mar. Biotechnol. 11 (4), 431–440. https://doi.org/10.1007/s10126-009-9191-4.
Chaussidon, M., Albarède, F., 1992. Secular boron isotope variations in the continental crust: an ion microprobe study. Earth Planet. Sci. Lett. 108 (4), 229–241. https://doi.org/10.1016/0012-821X(92)90025-Q.
Chaussidon, M., Jambon, A., 1994. Boron content and isotopic composition of oceanic basalts: geochemical and cosmochemical implications. Earth Planet. Sci. Lett. 121 (3–4), 277–291. https://doi.org/10.1016/0012-821X(94)90073-6.
Chetelat, B., Gaillardet, J., 2005. Boron isotopes in the Seine River, France: a probe of anthropogenic contamination. Environ. Sci. Technol. 39 (8), 2486–2493. https://doi.org/10.1021/Es048387j.
Chetelat, B., Gaillardet, J., Freydier, R., Negrel, P., 2005. Boron isotopes in precipitation: experimental constraints and field evidence from French Guiana. Earth Planet. Sci. Lett. 235 (1-2), 16–30. https://doi.org/10.1016/j.epsl.2005.02.014.
Chetelat, B., Gaillardet, J., Freydier, R., 2009a. Use of B isotopes as a tracer of anthropogenic emissions in the atmosphere of Paris. France. Appl. Geochem. 24 (5), 810–820. https://doi.org/10.1016/j.apgeochem.2009.01.007.
Chetelat, B., Liu, C.Q., Gaillardet, J., Wang, Q.L., Zhao, Z.Q., Liang, C.S., Xiao, Y.K., 2009b. Boron isotopes geochemistry of the Changjiang basin rivers. Geochim. Cosmochim. Acta 73 (20), 6084–6097. https://doi.org/10.1016/j.gca.2009.07.026.
Cividini, D., Lemarchand, D., Chabaux, F., Boutin, R., Pierret, M.C., 2010. From biological to lithological control of the B geochemical cycle in a forest watershed (Strengbach, Vosges). Geochim. Cosmochim. Acta 74 (11), 3143–3163. https://doi.org/10.1016/j.gca.2010.03.002.
Clauer, N., Williams, L.B., Lemarchand, D., Florian, P., Honty, M., 2018. Illitization decrypted by B and Li isotope geochemistry of nanometer-sized illite crystals from bentonite beds, East Slovak Basin. Chem. Geol. 477, 177–194. https://doi.org/10.1016/j.chemgeo.2017.10.027.
Coadic, R., Bassinot, F., Douville, E., Michel, E., Dissard, D., Greaves, M., 2013. A core-top study of dissolution effect on B/Ca in Globigerinoides sacculifer from the tropical Atlantic: potential bias for paleo-reconstruction of seawater carbonate chemistry. Geochem. Geophys. Geosyst. 14 (4), 1053–1068. https://doi.org/10.1029/2012gc004296.
Cody, R.D., 1970. Anomalous boron content of two continental shales in eastern Colorado. J. Sediment. Petrol. 40 (2), 750–754. https://doi.org/10.1306/74D72036-2B21-11D7-8648000102C1865D.
Davidson, G.R., Bassett, R.L., 1993. Application of boron isotopes for identifying contaminants such as fly-ash leachate in groundwater. Environ. Sci. Technol. 27 (1), 172–176. https://doi.org/10.1021/es00038a020.
de Hoog, J.C.M., Savov, I.P., 2018. Boron isotopes as a tracer of subduction zone processes. In: Marschall, H., Foster, G. (Eds.), Boron Isotopes: The Fifth Element. Springer International Publishing, Cham, pp. 217–247.
Dellinger, M., Gaillardet, J., Bouchez, J., Calmels, D., Louvat, P., Dosseto, A., Gorge, C., Alanoca, L., Maurice, L., 2015. Riverine Li isotope fractionation in the Amazon River basin controlled by the weathering regimes. Geochim. Cosmochim. Acta 164, 71–93. https://doi.org/10.1016/j.gca.2015.04.042.
Deyhle, A., Kopf, A.J., 2005. The use and usefulness of boron isotopes in natural silicate-water systems. Phys. Chem. Earth 30 (17-18), 1038–1046. https://doi.org/10.1016/j.pce.2005.04.003.
Dixon, J.L., Heimsath, A.M., Amundson, R., 2009. The critical role of climate and saprolite weathering in landscape evolution. Earth Surf. Process. Landf. 34 (11), 1507–1521. https://doi.org/10.1002/esp.1836.
Dixon, J.L., Hartshorn, A.S., Heimsath, A.M., DiBiase, R.A., Whipple, K.X., 2012. Chemical weathering response to tectonic forcing: a soils perspective from the San Gabriel Mountains, California. Earth Planet. Sci. Lett. 323–324, 40–49. https://doi.org/10.1016/j.epsl.2012.01.010.
Dominguez-Villar, D., Vazquez-Navarro, J.A., Krklec, K., 2017. The role of gypsum and/or dolomite dissolution in tufa precipitation: lessons from the hydrochemistry of a carbonate-sulphate karst system. Earth Surf. Process. Landf. 42 (2), 245–258. https://doi.org/10.1002/esp.3978.
Drivenes, K., Larsen, R.B., Müller, A., Sørensen, B.E., Wiedenbeck, M., Raanes, M.P., 2015. Late-magmatic immiscibility during batholith formation: assessment of B isotopes and trace elements in tourmaline from the Land's End granite. SW England. Contrib. Mineral. Petrol. 169 (6), 1–27. https://doi.org/10.1007/s00410-015-1151-6.
Durr, H.H., Meybeck, M., Durr, S.H., 2005. Lithologic composition of the Earth's continental surfaces derived from a new digital map emphasizing riverine material transfer. Glob. Biogeochem. Cycles 19https://doi.org/10.1029/2005gb002515. GB4S10.
Edgar, K.M., Anagnostou, E., Pearson, P.N., Foster, G.L., 2015. Assessing the impact of diagenesis on $\delta^{11}B$, $\delta^{13}C$, $\delta^{18}O$, Sr/Ca and B/Ca values in fossil planktic foraminiferal calcite. Geochim. Cosmochim. Acta 166, 189–209. https://doi.org/10.1016/j.gca.2015.06.018.
Engle, M.A., Reyes, F.R., Varonka, M.S., Orem, W.H., Ma, L., Ianno, A.J., Schell, T.M., Xu, P., Carroll, K.C., 2016. Geochemistry of formation waters from the Wolfcamp and "Cline" shales: insights into brine origin, reservoir connectivity, and fluid flow in the Permian Basin, USA. Chem. Geol. 425, 76–92. https://doi.org/10.1016/j.chemgeo.2016.01.025.
Fan, Q.S., Ma, Y.Q., Cheng, H.D., Wei, H.C., Yuan, Q., Qin, Z.J., Shan, F.S., 2015. Boron occurrence in halite and boron isotope geochemistry of halite in the Qarhan Salt Lake, western China. Sediment. Geol. 322, 34–42. https://doi.org/10.1016/j.sedgeo.2015.03.012.
Farber, E., Vengosh, A., Gavrieli, I., Marie, A., Bullen, T.D., Mayer, B., Holtzman, R., Segal, M., Shavit, U., 2004. The origin and mechanisms of salinization of the Lower Jordan River. Geochim. Cosmochim. Acta 68 (9), 1989–2006. https://doi.org/10.1016/j.gca.2003.09.021.
Farmer, G.L., 2014. 4.3 – Continental basaltic rocks. In: Holland, H.D., Turekian, K.K. (Eds.), Treatise on Geochemistry, Second Edition. Elsevier, Oxford, pp. 75–110.
Ferrier, K.L., Kirchner, J.W., 2008. Effects of physical erosion on chemical denudation rates: a numerical modeling study of soil-mantled hillslopes. Earth Planet. Sci. Lett. 272 (3-4), 591–599. https://doi.org/10.1016/j.epsl.2008.05.024.
Ferrier, K.L., Kirchner, J.W., Finkel, R.C., 2012. Weak influences of climate and mineral supply rates on chemical erosion rates: measurements along two altitudinal transects in the Idaho Batholith. J. Geophys. Res. Earth Surf. 117, F02026. https://doi.org/10.1029/2011JF002231.
Ferrier, K.L., Riebe, C.S., Hahm, W.J., 2016. Testing for supply-limited and kinetic-limited chemical erosion in field measurements of regolith production and chemical depletion. Geochem. Geophys. Geosyst. 17 (6), 2270–2285. https://doi.org/10.1002/2016gc006273.
Fogg, T.R., Duce, R.A., 1985. Boron in the troposphere: distribution and fluxes. J. Geophys. Res. Atmos. 90 (D2), 3781–3796. https://doi.org/10.1029/JD090iD02p03781.
Foster, G.L., 2008. Seawater pH, pCO_2 and $[CO_3^{2-}]$ variations in the Caribbean Sea over the last 130 kyr: a boron isotope and B/Ca study of planktic forminifera. Earth Planet. Sci. Lett. 271 (1-4), 254–266. https://doi.org/10.1016/j.epsl.2008.04.015.
Foster, G.L., Rae, J.W.B., 2016. Reconstructing ocean pH with boron isotopes in foraminifera. Annu. Rev. Earth Planet. Sci. 44 (1), 207–237. https://doi.org/10.1146/annurev-earth-060115-012226.
Foster, G.L., Pogge von Strandmann, P.A.E., Rae, J.W.B., 2010. Boron and magnesium isotopic composition of seawater. Geochem. Geophys. Geosyst. 11, Q08015. https://doi.org/10.1029/2010gc003201.
Gaillardet, J., Allegre, C.J., 1995. Boron isotopic compositions of corals: seawater or diagenesis record? Earth Planet. Sci. Lett. 136 (3-4), 665–676. https://doi.org/10.1016/0012-821x(95)00180-k.
Gaillardet, J., Lemarchand, D., 2018. Boron in the weathering environment. In: Marschall, H., Foster, G. (Eds.), Boron Isotopes: The Fifth Element. Springer International Publishing, Cham, pp. 163–188.
Gaillardet, J., Dupre, B., Louvat, P., Allegre, C.J., 1999. Global silicate weathering and CO_2 consumption rates deduced from the chemistry of large rivers. Chem. Geol. 159 (1-4), 3–30. https://doi.org/10.1016/S0009-2541(99)00031-5.
Gaillardet, J., Lemarchand, D., Gopel, C., Manhes, G., 2001. Evaporation and sublimation of boric acid: application for boron purification from organic rich solutions. Geostand. Newslett. 25 (1), 67–75. https://doi.org/10.1111/j.1751-908X.2001.tb00788.x.
Geilert, S., Vogl, J., Rosner, M., Voerkelius, S., Eichert, T., 2015. Boron isotope fractionation in bell pepper. Mass Spectrom. Purif. Tech. 1 (101). https://doi.org/10.4172/2469-9861.1000101.
Genske, F.S., Turner, S.P., Beier, C., Chu, M.F., Tonarini, S., Pearson, N.J., Haase, K.M., 2014. Lithium and boron isotope systematics in lavas from the Azores islands reveal crustal assimilation. Chem. Geol. 373, 27–36. https://doi.org/10.1016/j.chemgeo.2014.02.024.
Godderis, Y., Donnadieu, Y., Carretier, S., Aretz, M., Dera, G., Macouin, M., Regard, V., 2017. Onset and ending of the late Palaeozoic ice age triggered by tectonically paced rock weathering. Nat. Geosci. 10 (5), 382–386. https://doi.org/10.1038/ngeo2931.
Goldberg, S., 1997. Reactions of boron with soils. Plant Soil 193 (1-2), 35–48. https://doi.org/10.1023/A:1004203723343.
Goldberg, S., Glaubig, R.A., 1986. Boron adsorption and silicon release by the clay-minerals kaolinite, montmorillonite, and illite. Soil Sci. Soc. Am. J. 50 (6), 1442–1448. https://doi.org/10.2136/sssaj1986.03615995005000060013x.
Goldberg, S., Su, C., 2007. New advances in boron soil chemistry. In: Xu, F., Goldbach, H.E., Brown, P.H., Bell, R.W., Fujiwara, T., Hunt, C.D., Goldberg, S., Shi, L.E.I. (Eds.), Advances in Plant and Animal Boron Nutrition. Springer Netherlands, Dordrecht, pp. 313–330.
Grew, E.S., 2015. Boron – the crustal element. Elements 11 (3), 162–163.
Guerrot, C., Millot, R., Robert, M., Negrel, P., 2011. Accurate and high-precision determination of boron isotopic ratios at low concentration by MC-ICP-MS (Neptune). Geostand. Geoanal. Res. 35 (2), 275–284. https://doi.org/10.1111/j.1751-908X.2010.00073.x.
Guinoiseau, D., Louvat, P., Paris, G., Chen, J.-B., Chetelat, B., Rocher, V., Guérin, S., Gaillardet, J., 2018. Are boron isotopes a reliable tracer of anthropogenic inputs to rivers over time? Sci. Total Environ. 626, 1057–1068. https://doi.org/10.1016/j.scitotenv.2018.01.159.
Harder, H., 1970. Boron content of sediments as a tool in facies analysis. Sediment. Geol. 4 (2), 153–175. https://doi.org/10.1016/0037-0738(70)90009-6.

Harkness, J.S., Sulkin, B., Vengosh, A., 2016. Evidence for coal ash ponds leaking in the Southeastern United States. Environ. Sci. Technol. 50 (12), 6583–6592. https://doi.org/10.1021/acs.est.6b01727.
Hartmann, J., Moosdorf, N., 2012. The new global lithological map database GLiM: a representation of rock properties at the Earth surface. Geochem. Geophys. Geosyst. 13, Q12004. https://doi.org/10.1029/2012gc004370.
Harvey, J., Garrido, C.J., Savov, I., Agostini, S., Padron-Navarta, J.A., Marchesi, C., Sanchez-Vizcaino, V.L., Gomez-Pugnaire, M.T., 2014a. ^{11}B-rich fluids in subduction zones: the role of antigorite dehydration in subducting slabs and boron isotope heterogeneity in the mantle. Chem. Geol. 376, 20–30. https://doi.org/10.1016/j.chemgeo.2014.03.015.
Harvey, J., Savov, I.P., Agostini, S., Cliff, R.A., Walshaw, R., 2014b. Si-metasomatism in serpentinized peridotite: the effects of talc-alteration on strontium and boron isotopes in abyssal serpentinites from Hole 1268a, ODP Leg 209. Geochim. Cosmochim. Acta 126, 30–48. https://doi.org/10.1016/j.gca.2013.10.035.
Hemming, N.G., Hanson, G.N., 1992. Boron isotopic composition and concentration in modern marine carbonates. Geochim. Cosmochim. Acta 56 (1), 537–543. https://doi.org/10.1016/0016-7037(92)90151-8.
Hemming, N.G., Reeder, R.J., Hanson, G.N., 1995. Mineral-fluid partitioning and isotopic fractionation of boron in synthetic calcium carbonate. Geochim. Cosmochim. Acta 59 (2), 371–379. https://doi.org/10.1016/0016-7037(95)00288-B.
Henehan, M.J., Foster, G.L., Bostock, H.C., Greenop, R., Marshall, B.J., Wilson, P.A., 2016. A new boron isotope-pH calibration for Orbulina universa, with implications for understanding and accounting for "vital effects". Earth Planet. Sci. Lett. 454, 282–292. https://doi.org/10.1016/j.epsl.2016.09.024.
Hobbs, M.Y., Reardon, E.J., 1999. Effect of pH on boron coprecipitation by calcite: further evidence for nonequilibrium partitioning of trace elements. Geochim. Cosmochim. Acta 63 (7-8), 1013–1021. https://doi.org/10.1016/S0016-7037(98)00311-1.
Hogan, J.F., Blum, J.D., 2003. Boron and lithium isotopes as groundwater tracers: a study at the Fresh Kills Landfill, Staten Island, New York, USA. Appl. Geochem. 18 (4), 615–627. https://doi.org/10.1016/S0883-2927(02)00153-1.
Ilgen, A.G., Heath, J.E., Yucel Akkutlu, I., Taras Bryndzia, L., Cole, D.R., Kharaka, Y.K., Kneafsey, T.J., Milliken, K.L., Pyrak-Nolte, L.J., Suarez-Rivera, R., 2017. Shales at all scales: exploring coupled processes in mudrocks. Earth Sci. Rev. 166, 132–152. https://doi.org/10.1016/j.earscirev.2016.12.013.
Ishikawa, T., Nakamura, E., 1992. Boron isotope geochemistry of the oceanic crust from DSDP/ODP Hole 504B. Geochim. Cosmochim. Acta 56 (4), 1633–1639. https://doi.org/10.1016/0016-7037(92)90230-G.
Ishikawa, T., Nakamura, E., 1993. Boron isotope systematics of marine sediments. Earth Planet. Sci. Lett. 117 (3-4), 567–580. https://doi.org/10.1016/0012-821x(93)90103-g.
Jiang, S.Y., 2001. Boron isotope geochemistry of hydrothermal ore deposits in China: a preliminary study. Phys. Chem. Earth Solid Earth Geod. 26 (9), 851–858. https://doi.org/10.1016/S1464-1895(01)00132-6.
Jiang, S.Y., Palmer, M.R., 1998. Boron isotope systematics of tourmaline from granites and pegmatites: a synthesis. Eur. J. Mineral. 10 (6), 1253–1265. https://doi.org/10.1127/ejm/10/6/1253.
Jiang, S.Y., Palmer, M.R., Peng, Q.M., Yang, J.H., 1997. Chemical and stable isotopic compositions of Proterozoic metamorphosed evaporites and associated tourmalines from the Houxianyu borate deposit, eastern Liaoning, China. Chem. Geol. 135 (3-4), 189–211. https://doi.org/10.1016/s0009-2541(96)00115-5.
Joachimski, M.M., Simon, L., van Geldern, R., Lecuyer, C., 2005. Boron isotope geochemistry of Paleozoic brachiopod calcite: implications for a secular change in the boron isotope geochemistry of seawater over the Phanerozoic. Geochim. Cosmochim. Acta 69 (16), 4035–4044. https://doi.org/10.1016/j.gca.2004.11.017.
Kaczmarek, K., Nehrke, G., Misra, S., Bijma, J., Elderfield, H., 2016. Investigating the effects of growth rate and temperature on the B/Ca ratio and delta B-11 during inorganic calcite formation. Chem. Geol. 421, 81–92. https://doi.org/10.1016/j.chemgeo.2015.12.002.
Kaliwoda, M., Marschall, H.R., Marks, M.A.W., Ludwig, T., Altherr, R., Markl, G., 2011. Boron and boron isotope systematics in the peralkaline Ilimaussaq intrusion (South Greenland) and its granitic country rocks: a record of magmatic and hydrothermal processes. Lithos 125 (1-2), 51–64. https://doi.org/10.1016/j.lithos.2011.01.006.
Keren, R., Mezuman, U., 1981. Boron adsorption by clay-minerals using a phenomenological equation. Clay Clay Miner. 29 (3), 198–204. https://doi.org/10.1346/Ccmn.1981.0290305.
Keren, R., Talpaz, H., 1984. Boron adsorption by montmorillonite as affected by particle size. Soil Sci. Soc. Am. J. 48 (3), 555–559. https://doi.org/10.2136/sssaj1984.03615995004800030017x.
Kitano, Y., Okumura, M., Idogaki, M., 1978. Coprecipitation of borate-boron with calcium carbonate. Geochem. J. 12 (3), 183–189. https://doi.org/10.2343/geochemj.12.183.
Kobayashi, K., Tanaka, R., Moriguti, T., Shimizu, K., Nakamura, E., 2004. Lithium, boron, and lead isotope systematics of glass inclusions in olivines from Hawaiian lavas: evidence for recycled components in the Hawaiian plume. Chem. Geol. 212 (1–2), 143–161. https://doi.org/10.1016/j.chemgeo.2004.08.050.
Komor, S.C., 1997. Boron contents and isotopic compositions of hog manure, selected fertilizers, and water in Minnesota. J. Environ. Qual. 26 (5), 1212–1222. https://doi.org/10.2134/jeq1997.00472425002600050004x.
Konrad-Schmolke, M., Halama, R., 2014. Combined thermodynamic-geochemical modeling in metamorphic geology: boron as tracer of fluid-rock interaction. Lithos 208, 393–414. https://doi.org/10.1016/j.lithos.2014.09.021.
Konrad-Schmolke, M., Halama, R., Manea, V.C., 2016. Slab mantle dehydrates beneath Kamchatka–Yet recycles water into the deep mantle. Geochem. Geophys. Geosyst. 17 (8), 2987–3007. https://doi.org/10.1002/2016GC006335.
Kot, F.S., 2015. Chapter 1 – boron in the environment. In: Kabay, N., Bryjak, M., Hilal, N. (Eds.), Boron Separation Processes. Elsevier, Amsterdam, pp. 1–33.
Kozdon, R., Kelly, D.C., Kitajima, K., Strickland, A., Fournelle, J.H., Valley, J.W., 2013. In situ δ^{18}O and Mg/Ca analyses of diagenetic and planktic foraminiferal calcite preserved in a deep-sea record of the Paleocene-Eocene thermal maximum. Paleoceanography 28 (3), 517–528. https://doi.org/10.1002/palo.20048.
Lambert-Smith, J.S., Rocholl, A., Treloar, P.J., Lawrence, D.M., 2016. Discriminating fluid source regions in orogenic gold deposits using B-isotopes. Geochim. Cosmochim. Acta 194, 57–76. https://doi.org/10.1016/j.gca.2016.08.025.
Leeman, W.P., Sisson, V.B., 1996. Geochemistry of boron and its implications for crustal and mantle processes. In: Grew, E.S., Anovitz, L.M. (Eds.), Boron: Mineralogy, Petrology and Geochemistry. Mineral. Soc. Am.pp. 645–707.
Lemarchand, D., Gaillardet, J., 2006. Transient features of the erosion of shales in the Mackenzie basin (Canada), evidences from boron isotopes. Earth Planet. Sci. Lett. 245 (1-2), 174–189. https://doi.org/10.1016/j.cpsl.2006.01.056.
Lemarchand, D., Gaillardet, J., Lewin, E., Allegre, C.J., 2000. The influence of rivers on marine boron isotopes and implications for reconstructing past ocean pH. Nature 408 (6815), 951–954. https://doi.org/10.1038/35050058.
Lemarchand, D., Gaillardet, J., Gopel, C., Manhes, G., 2002a. An optimized procedure for boron separation and mass spectrometry analysis for river samples. Chem. Geol. 182 (2-4), 323–334. https://doi.org/10.1016/S0009-2541(01)00329-1.
Lemarchand, D., Gaillardet, J., Lewin, E., Allegre, C.J., 2002b. Boron isotope systematics in large rivers: implications for the marine boron budget and paleo-pH reconstruction over the Cenozoic. Chem. Geol. 190 (1-4), 123–140. https://doi.org/10.1016/s0009-2541(02)00114-6.
Lemarchand, E., Schott, J., Gaillardet, J., 2005. Boron isotopic fractionation related to boron sorption on humic acid and the structure of surface complexes formed. Geochim. Cosmochim. Acta 69 (14), 3519–3534. https://doi.org/10.1016/j.gca.2005.02.024.
Lemarchand, E., Schott, J., Gaillardet, J., 2007. How surface complexes impact boron isotope fractionation: evidence from Fe and Mn oxides sorption experiments. Earth Planet. Sci. Lett. 260 (1-2), 277–296. https://doi.org/10.1016/j.epsl.2007.05.039.
Lemarchand, D., Cividini, D., Turpault, M.P., Chabaux, F., 2012. Boron isotopes in different grain size fractions: exploring past and present water-rock interactions from two soil profiles (Strengbach, Vosges Mountains). Geochim. Cosmochim. Acta 98, 78–93. https://doi.org/10.1016/j.gca.2012.09.009.
Lemarchand, D., Jacobson, A.D., Cividini, D., Chabaux, F., 2015. The major ion, ^{87}Sr/^{86}Sr, and δ^{11}B geochemistry of groundwater in the Wyodak-Anderson coal bed aquifer (Powder River Basin, Wyoming, USA). Compt. Rendus Geosci. 347 (7–8), 348–357. https://doi.org/10.1016/j.crte.2015.05.007.
Li, S.-L., Liu, C.-Q., Li, J., Lang, Y.-C., Ding, H., Li, L., 2010. Geochemistry of dissolved inorganic carbon and carbonate weathering in a small typical karstic catchment of Southwest China: isotopic and chemical constraints. Chem. Geol. 277 (3–4), 301–309. https://doi.org/10.1016/j.chemgeo.2010.08.013.
Li, H.-Y., Zhou, Z., Ryan, J.G., Wei, G.-J., Xu, Y.-G., 2016. Boron isotopes reveal multiple metasomatic events in the mantle beneath the eastern North China Craton. Geochim. Cosmochim. Acta 194, 77–90. https://doi.org/10.1016/j.gca.2016.08.027.
Liu, Y., Tossell, J.A., 2005. Ab initio molecular orbital calculations for boron isotope fractionations on boric acids and borates. Geochim. Cosmochim. Acta 69 (16), 3995–4006. https://doi.org/10.1016/j.gca.2005.04.009.
Liu, W.G., Xiao, Y.K., Peng, Z.C., An, Z.S., He, X.X., 2000. Boron concentration and isotopic composition of halite from experiments and salt lakes in the Qaidam Basin. Geochim. Cosmochim. Acta 64 (13), 2177–2183. https://doi.org/10.1016/s0016-7037(00)00363-x.
Liu, Y.C., You, C.F., Huang, K.F., Wang, R.M., Chung, C.H., Liu, H.C., 2012. Boron sources and transport mechanisms in river waters collected from southwestern Taiwan: isotopic evidence. J. Asian Earth Sci. 58, 16–23. https://doi.org/10.1016/j.jseaes.2012.07.008.
Liu, H.C., You, C.F., Chen, C.Y., Liu, Y.C., Chung, M.T., 2014. Geographic determination of coffee beans using multi-element analysis and isotope ratios of boron and strontium. Food Chem. 142, 439–445. https://doi.org/10.1016/j.foodchem.2013.07.082.
London, D., Morgan, G.B., Wolf, M.B., 1996. Boron in granitic rocks and their contact aureoles. In: Grew, E.S., Anovitz, L.M. (Eds.), Boron: Mineralogy, Petrology and Geochemistry. Mineral. Soc. Am.pp. 299–325.
Louvat, P., Bouchez, J., Paris, G., 2011a. MC-ICP-MS isotope measurements with direct injection nebulisation (d-DIHEN): optimisation and application to boron in seawater and carbonate samples. Geostand. Geoanal. Res. 35 (1), 75–88. https://doi.org/10.1111/j.1751-908X.2010.00057.x.
Louvat, P., Gaillardet, J., Paris, G., Dessert, C., 2011b. Boron isotope ratios of surface waters in Guadeloupe, Lesser Antilles. Appl. Geochem. 26, S76–S79. https://doi.org/10.1016/j.apgeochem.2011.03.035.
Louvat, P., Gayer, E., Gaillardet, J., 2014. Boron behavior in the rivers of Réunion island, inferred from boron isotope ratios and concentrations of major and trace elements. Procedia Earth Planet. Sci. 10, 231–237. https://doi.org/10.1016/j.proeps.2014.08.029.
MacGregor, J., Grew, E.S., De Hoog, J.C.M., Harley, S.L., Kowalski, P.M., Yates, M.G., Carson, C.J., 2013. Boron isotopic composition of tourmaline, prismatine, and grandidierite from granulite facies paragneisses in the Larsemann Hills, Prydz Bay, East Antarctica: evidence for a non-marine evaporite source. Geochim. Cosmochim. Acta 123, 261–283. https://doi.org/10.1016/j.gca.2013.05.030.
Maher, K., Chamberlain, C.P., 2014. Hydrologic regulation of chemical weathering and the geologic carbon cycle. Science 343 (6178), 1502–1504. https://doi.org/10.1126/science.1250770.
Manea, V.C., Leeman, W.P., Gerya, T., Manea, M., Zhu, G., 2014. Subduction of fracture zones controls mantle melting and geochemical signature above slabs. Nat. Commun. 5, 5095. https://doi.org/10.1038/ncomms6095.
Marschall, H.R., 2018. Boron isotopes in the ocean floor realm and the mantle. In: Marschall, H., Foster, G. (Eds.), Boron Isotopes: The Fifth Element. Springer

International Publishing, Cham, pp. 189–215.
Marschall, H.R., Foster, G.L., 2018. Boron isotopes in the earth and planetary sciences—a short history and introduction. In: Marschall, H., Foster, G. (Eds.), Boron Isotopes: The Fifth Element. Springer International Publishing, Cham, pp. 1–11.
Marschall, H.R., Jiang, S.Y., 2011. Tourmaline isotopes: no element left behind. Elements 7 (5), 313–319. https://doi.org/10.2113/gselements.7.5.313.
Marschall, H.R., Monteleone, B.D., 2015. Boron isotope analysis of silicate glass with very low boron concentrations by secondary ion mass spectrometry. Geostand. Geoanal. Res. 39 (1), 31–46. https://doi.org/10.1111/j.1751-908X.2014.00289.x.
Marschall, H.R., Ludwig, T., Altherr, R., Kalt, A., Tonarini, S., 2006. Syros metasomatic tourmaline: evidence for very high-delta B-11 fluids in subduction zones. J. Petrol. 47 (10), 1915–1942. https://doi.org/10.1093/petrology/egl031.
Marschall, H.R., Altherr, R., Rüpke, L., 2007. Squeezing out the slab – modelling the release of Li, Be and B during progressive high-pressure metamorphism. Chem. Geol. 239 (3–4), 323–335. https://doi.org/10.1016/j.chemgeo.2006.08.008.
Marschall, H.R., Meyer, C., Wunder, B., Ludwig, T., Heinrich, W., 2009. Experimental boron isotope fractionation between tourmaline and fluid: confirmation from in situ analyses by secondary ion mass spectrometry and from Rayleigh fractionation modelling. Contrib. Mineral. Petrol. 158 (5), 675–681. https://doi.org/10.1007/s00410-009-0403-8.
Marschall, H.R., Dorsey Wanless, V., Shimizu, N., Pogge von Strandmann, P.A.E., Elliott, T., Monteleone, B.D., 2017. The boron and lithium isotopic composition of mid-ocean ridge basalts and the mantle. Geochim. Cosmochim. Acta 207, 102–138. https://doi.org/10.1016/j.gca.2017.03.028.
Martens, C.S., Harriss, R.C., 1976. Boron in coastal North Florida rainfall. J. Geophys. Res. Oceans Atmos. 81 (36), 6371–6375. https://doi.org/10.1029/JC081i036p06371.
Mather, J.D., Porteous, N.C., 2001. The geochemistry of boron and its isotopes in groundwaters from marine and non-marine sandstone aquifers. Appl. Geochem. 16 (7-8), 821–834. https://doi.org/10.1016/s0883-2927(00)00072-x.
Mattigod, S.V., Frampton, J.A., Lim, C.H., 1985. Effect of ion-pair formation on boron adsorption by kaolinite. Clay Clay Miner. 33 (5), 433–437. https://doi.org/10.1346/Ccmn.1985.0330509.
Mavromatis, V., Montouillout, V., Noireaux, J., Gaillardet, J., Schott, J., 2015. Characterization of boron incorporation and speciation in calcite and aragonite from co-precipitation experiments under controlled pH, temperature and precipitation rate. Geochim. Cosmochim. Acta 150, 299–313. https://doi.org/10.1016/j.gca.2014.10.024.
Metrich, N., Deloule, E., 2014. Water content, δD and $\delta^{11}B$ tracking in the Vanuatu arc magmas (Aoba Island): insights from olivine-hosted melt inclusions. Lithos 206, 400–408. https://doi.org/10.1016/j.lithos.2014.08.011.
Meybeck, M., 1987. Global chemical weathering of surficial rocks estimated from river dissolved loads. Am. J. Sci. 287 (5), 401–428. https://doi.org/10.2475/ajs.287.5.401.
Millot, R., Petelet-Giraud, E., Guerrot, C., Negrel, P., 2010. Multi-isotopic composition (δ^7Li-δ^{11}B-δD-δ^{18}O) of rainwaters in France: origin and spatio-temporal characterization. Appl. Geochem. 25 (10), 1510–1524. https://doi.org/10.1016/j.apgeochem.2010.08.002.
Miyata, Y., Tokieda, T., Amakawa, H., Uematsu, M., Nozaki, Y., 2000. Boron isotope variations in the atmosphere. Tellus Ser. B Chem. Phys. Meteorol. 52 (4), 1057–1065. https://doi.org/10.1034/j.1600-0889.2000.00089.x.
Moran, A.E., Sisson, V.B., Leeman, W.P., 1992. Boron depletion during progressive metamorphism: implications for subduction processes. Earth Planet. Sci. Lett. 111 (2-4), 331–349. https://doi.org/10.1016/0012-821x(92)90188-2.
Muttik, N., Kirsimae, K., Newsom, H.E., Williams, L.B., 2011. Boron isotope composition of secondary smectite in suevites at the Ries crater, Germany: boron fractionation in weathering and hydrothermal processes. Earth Planet. Sci. Lett. 310 (3-4), 244–251. https://doi.org/10.1016/j.epsl.2011.08.028.
Nakano, T., Nakamura, E., 2001. Boron isotope geochemistry of metasedimentary rocks and tourmalines in a subduction zone metamorphic suite. Phys. Earth Planet. Inter. 127 (1–4), 233–252. https://doi.org/10.1016/S0031-9201(01)00230-8.
Noireaux, J., Gaillardet, J., Sullivan, P.L., Brantley, S.L., 2014. Boron isotope fractionation in soils at Shale Hills CZO. Procedia Earth Planet. Sci. 10, 218–222. https://doi.org/10.1016/j.proeps.2014.08.024.
Noireaux, J., Mavromatis, V., Gaillardet, J., Schott, J., Montouillout, V., Louvat, P., Rollion-Bard, C., Neuville, D.R., 2015. Crystallographic control on the boron isotope paleo-pH proxy. Earth Planet. Sci. Lett. 430, 398–407. https://doi.org/10.1016/j.epsl.2015.07.063.
Oi, T., Nomura, M., Musashi, M., Ossaka, T., Okamoto, M., Kakihana, H., 1989. Boron isotopic compositions of some boron minerals. Geochim. Cosmochim. Acta 53 (12), 3189–3195. https://doi.org/10.1016/0016-7037(89)90099-9.
Palmer, M.R., 2017. Boron cycling in subduction zones. Elements 13 (4), 237–242. https://doi.org/10.2138/gselements.13.4.237.
Palmer, M.R., Helvaci, C., 1995. The boron isotope geochemistry of the Kirka borate deposit, western Turkey. Geochim. Cosmochim. Acta 59 (17), 3599–3605. https://doi.org/10.1016/0016-7037(95)00227-Q.
Palmer, M.R., Helvaci, C., 1997. The boron isotope geochemistry of the neogene borate deposits of western Turkey. Geochim. Cosmochim. Acta 61 (15), 3161–3169. https://doi.org/10.1016/S0016-7037(97)00135-X.
Palmer, M.R., Swihart, G.R., 1996. Boron isotope geochemistry: an overview. In: Grew, E.S., Anovitz, L.M. (Eds.), Boron: Mineralogy, Petrology and Geochemistry. Mineral. Soc. Am.pp. 709–744.
Palmer, M.R., Spivack, A.J., Edmond, J.M., 1987. Temperature and pH controls over isotopic fractionation during adsorption of boron on marine clay. Geochim. Cosmochim. Acta 51 (9), 2319–2323. https://doi.org/10.1016/0016-7037(87)90285-7.
Paris, G., Bartolini, A., Donnadieu, Y., Beaumont, V., Gaillardet, J., 2010a. Investigating boron isotopes in a middle Jurassic micritic sequence: primary vs. diagenetic signal. Chem. Geol. 275 (3-4), 117–126. https://doi.org/10.1016/j.chemgeo.2010.03.013.
Paris, G., Gaillardet, J., Louvat, P., 2010b. Geological evolution of seawater boron isotopic composition recorded in evaporites. Geology 38 (11), 1035–1038. https://doi.org/10.1130/g31321.1.
Park, H., Schlesinger, W.H., 2002. Global biogeochemical cycle of boron. Glob. Biogeochem. Cycles 16 (4), 1072. https://doi.org/10.1029/2001gb001766.
Peacock, S.M., Hervig, R.L., 1999. Boron isotopic composition of subduction-zone metamorphic rocks. Chem. Geol. 160 (4), 281–290. https://doi.org/10.1016/S0009-2541(99)00103-5.
Penman, D.E., Honisch, B., Zeebe, R.E., Thomas, E., Zachos, J.C., 2014. Rapid and sustained surface ocean acidification during the Paleocene-Eocene Thermal Maximum. Paleoceanography 29 (5), 357–369. https://doi.org/10.1002/2014PA002621.
Pennisi, M., Bianchini, G., Kloppmann, W., Muti, A., 2009. Chemical and isotopic (B, Sr) composition of alluvial sediments as archive of a past hydrothermal outflow. Chem. Geol. 266 (3-4), 114–125. https://doi.org/10.1016/j.chemgeo.2009.05.017.
Petelet-Giraud, E., Négrel, P., Guerrot, C., 2015. Boron isotope variation during flood events in a Mediterranean basin: tracer of the water compartments (Hérault, S. France). Procedia Earth Planet. Sci. 13, 203–206. https://doi.org/10.1016/j.proeps.2015.07.048.
Pi, J.L., You, C.F., Chung, C.H., 2014. Micro-sublimation separation of boron in rock samples for isotopic measurement by MC-ICPMS. J. Anal. At. Spectrom. 29 (5), 861–867. https://doi.org/10.1039/c3ja50344e.
Plank, T., 2014. 4.17 – The chemical composition of subducting sediments A2 – Holland, Heinrich D. In: Turekian, K.K. (Ed.), Treatise on Geochemistry, Second Edition. Elsevier, Oxford, pp. 607–629.
Prigent, C., Guillot, S., Agard, P., Lemarchand, D., Soret, M., Ulrich, M., 2018. Transfer of subduction fluids into the deforming mantle wedge during nascent subduction: evidence from trace elements and boron isotopes (Semail ophiolite, Oman). Earth Planet. Sci. Lett. 484, 213–228. https://doi.org/10.1016/j.epsl.2017.12.008.
Puig, R., Soler, A., Widory, D., Mas-Pla, J., Domènech, C., Otero, N., 2017. Characterizing sources and natural attenuation of nitrate contamination in the Baix Ter aquifer system (NE Spain) using a multi-isotope approach. Sci. Total Environ. 580, 518–532. https://doi.org/10.1016/j.scitotenv.2016.11.206.
Qi, H.P., Wang, Y.H., Xiao, Y.K., Sun, D.P., Jin, L., Tang, Y., 1993. A preliminary investigation on the isotopic composition of boron in salt lakes of China. Chin. Sci. Bull. 38 (7), 634–637.
Rae, J.W.B., 2018. Boron isotopes in foraminifera: systematics, biomineralisation, and CO2 reconstruction. In: Marschall, H., Foster, G. (Eds.), Boron Isotopes: The Fifth Element. Springer International Publishing, Cham, pp. 107–143.
Regenberg, M., Nurnberg, D., Schonfeld, J., Reichart, G.J., 2007. Early diagenetic overprint in Caribbean sediment cores and its effect on the geochemical composition of planktonic foraminifera. Biogeosciences 4 (6), 957–973. https://doi.org/10.5194/bg-4-957-2007.
Reid, R., 2014. Understanding the boron transport network in plants. Plant Soil 385 (1-2), 1–13. https://doi.org/10.1007/s11104-014-2149-y.
Riebe, C.S., Kirchner, J.W., Granger, D.E., Finkel, R.C., 2001. Strong tectonic and weak climatic control of long-term chemical weathering rates. Geology 29 (6), 511–514. https://doi.org/10.1130/0091-7613(2001)029<0511:stawcc>2.0.co;2.
Riebe, C.S., Kirchner, J.W., Finkel, R.C., 2003. Long-term rates of chemical weathering and physical erosion from cosmogenic nuclides and geochemical mass balance. Geochim. Cosmochim. Acta 67 (22), 4411–4427. https://doi.org/10.1016/S0016-7037(03)00382-X.
Riebe, C.S., Kirchner, J.W., Finkel, R.C., 2004. Erosional and climatic effects on long-term chemical weathering rates in granitic landscapes spanning diverse climate regimes. Earth Planet. Sci. Lett. 224 (3–4), 547–562. https://doi.org/10.1016/j.epsl.2004.05.019.
Riebe, C.S., Hahm, W.J., Brantley, S.L., 2017. Controls on deep critical zone architecture: a historical review and four testable hypotheses. Earth Surf. Process. Landf. 42 (1), 128–156. https://doi.org/10.1002/esp.4052.
Romer, R.L., Meixner, A., 2014. Lithium and boron isotopic fractionation in sedimentary rocks during metamorphism – the role of rock composition and protolith mineralogy. Geochim. Cosmochim. Acta 128, 158–177. https://doi.org/10.1016/j.gca.2013.11.032.
Romer, R.L., Meixner, A., Forster, H.J., 2014a. Lithium and boron in late-orogenic granites – isotopic fingerprints for the source of crustal melts? Geochim. Cosmochim. Acta 131, 98–114. https://doi.org/10.1016/j.gca.2014.01.018.
Romer, R.L., Meixner, A., Hahne, K., 2014b. Lithium and boron isotopic composition of sedimentary rocks – the role of source history and depositional environment: a 250Ma record from the Cadomian orogeny to the Variscan orogeny. Gondwana Res. 26 (3-4), 1093–1110. https://doi.org/10.1016/j.gr.2013.08.015.
Rose, E.F., Carignan, J., Chaussidon, M., 2000a. Transfer of atmospheric boron from the oceans to the continents: an investigation using precipitation waters and epiphytic lichens. Geochem. Geophys. Geosyst. 1https://doi.org/10.1029/2000GC000077. 2000GC000077.
Rose, E.F., Chaussidon, M., France-Lanord, C., 2000b. Fractionation of Boron isotopes during erosion processes: the example of Himalayan rivers. Geochim. Cosmochim. Acta 64 (3), 397–408. https://doi.org/10.1016/s0016-7037(99)00117-9.
Rose-Koga, E.F., Sheppard, S.M.F., Chaussidon, M., Carignan, J., 2006. Boron isotopic composition of atmospheric precipitations and liquid-vapour fractionations. Geochim. Cosmochim. Acta 70 (7), 1603–1615. https://doi.org/10.1016/j.gca.2006.01.003.
Rosner, M., Pritzkow, W., Vogl, J., Voerkelius, S., 2011. Development and validation of a method to determine the boron isotopic composition of crop plants. Anal. Chem. 83 (7), 2562–2568. https://doi.org/10.1021/ac102836h.
Roux, P., Lemarchand, D., Hughes, H.J., Turpault, M.-P., 2015. A rapid method for

determining boron concentration (ID-ICP-MS) and δ11B (MC-ICP-MS) in vegetation samples after microwave digestion and cation exchange chemical purification. Geostand. Geoanal. Res. https://doi.org/10.1111/j.1751-908X.2014.00328.x.
Roux, P., Turpault, M.-P., Kirchen, G., Redon, P.-O., Lemarchand, D., 2017. Boron dissolved and particulate atmospheric inputs to a forest ecosystem (Northeastern France). Environ. Sci. Technol. 51 (24), 14038–14046. https://doi.org/10.1021/acs.est.7b03226.
Roy-Barman, M., Wasserburg, G.J., Papanastassiou, D.A., Chaussidon, M., 1998. Osmium isotopic compositions and Re–Os concentrations in sulfide globules from basaltic glasses. Earth Planet. Sci. Lett. 154 (1), 331–347. https://doi.org/10.1016/S0012-821X(97)00180-5.
Rudnick, R.L., Tomascak, P.B., Njo, H.B., Gardner, L.R., 2004. Extreme lithium isotopic fractionation during continental weathering revealed in saprolites from South Carolina. Chem. Geol. 212 (1–2), 45–57. https://doi.org/10.1016/j.chemgeo.2004.08.008.
Ruhl, L.S., Dwyer, G.S., Hsu-Kim, H., Hower, J.C., Vengosh, A., 2014. Boron and strontium isotopic characterization of coal combustion residuals: validation of new environmental tracers. Environ. Sci. Technol. 48 (24), 14790–14798. https://doi.org/10.1021/es503746v.
Ryan, J.G., Leeman, W.P., Morris, J.D., Langmuir, C.H., 1996. The boron systematics of intraplate lavas: implications for crust and mantle evolution. Geochim. Cosmochim. Acta 60 (3), 415–422. https://doi.org/10.1016/0016-7037(95)00402-5.
Sakata, M., Ishikawa, T., Mitsunobu, S., 2013. Effectiveness of sulfur and boron isotopes in aerosols as tracers of emissions from coal burning in Asian continent. Atmos. Environ. 67, 296–303. https://doi.org/10.1016/j.atmosenv.2012.11.025.
Saldi, G.D., Noireaux, J., Louvat, P., Faure, L., Balan, E., Schott, J., Gaillardet, J., 2018. Boron isotopic fractionation during adsorption by calcite – implication for the seawater pH proxy. Geochim. Cosmochim. Acta. https://doi.org/10.1016/j.gca.2018.08.025.
Sanyal, A., Nugent, M., Reeder, R.J., Buma, J., 2000. Seawater pH control on the boron isotopic composition of calcite: evidence from inorganic calcite precipitation experiments. Geochim. Cosmochim. Acta 64 (9), 1551–1555. https://doi.org/10.1016/S0016-7037(99)00437-8.
Scambelluri, M., Tonarini, S., 2012. Boron isotope evidence for shallow fluid transfer across subduction zones by serpentinized mantle. Geology 40 (10), 907–910. https://doi.org/10.1130/g33233.1.
Schlesinger, W.H., Vengosh, A., 2016. Global boron cycle in the anthropocene. Glob. Biogeochem. Cycles 30 (2). https://doi.org/10.1002/2015GB005266.
Schmitt, A.D., Vigier, N., Lemarchand, D., Millot, R., Stille, P., Chabaux, F., 2012. Processes controlling the stable isotope compositions of Li, B, Mg and Ca in plants, soils and waters: a review. Compt. Rendus Geosci. 344 (11-12), 704–722. https://doi.org/10.1016/j.crte.2012.10.002.
Schoonejans, J., Vanacker, V., Opfergelt, S., Ameijeiras-Mariño, Y., Christl, M., 2016. Kinetically limited weathering at low denudation rates in semiarid climatic conditions. J. Geophys. Res. Earth Surf. 121 (2), 336–350. https://doi.org/10.1002/2015JF003626.
Schwarcz, H.P., Agyei, E.K., McMullen, C.C., 1969. Boron isotopic fractionation during clay adsorption from sea-water. Earth Planet. Sci. Lett. 6 (1), 1–5. https://doi.org/10.1016/0012-821X(69)90084-3.
Serra, F., Guillou, C.G., Reniero, F., Ballarin, L., Cantagallo, M.I., Wieser, M., Iyer, S.S., Heberger, K., Vanhaecke, F., 2005. Determination of the geographical origin of green coffee by principal component analysis of carbon, nitrogen and boron stable isotope ratios. Rapid Commun. Mass Spectrom. 19 (15), 2111–2115. https://doi.org/10.1002/rcm.2034.
Shaw, D.M., Bugry, R., 1966. A review of boron sedimentary geochemistry in relation to new analyses of some North American shales. Can. J. Earth Sci. 3 (1), 49–63. https://doi.org/10.1139/e66-004.
Siegel, K., Wagner, T., Trumbull, R.B., Jonsson, E., Matalin, G., Walle, M., Heinrich, C.A., 2016. Stable isotope (B, H, O) and mineral-chemistry constraints on the magmatic to hydrothermal evolution of the Varutrask rare-element pegmatite (Northern Sweden). Chem. Geol. 421, 1–16. https://doi.org/10.1016/j.chemgeo.2015.11.025.
Singh, M., 1971. Equilibrium adsorption of boron in soils and clays. Geoderma 5 (3), 209–217. https://doi.org/10.1016/0016-7061(71)90010-3.
Singh, S.P., Singh, S.K., Bhushan, R., 2014. Dissolved Boron in the Tapi, Narmada and the Mandovi estuaries, the western coast of India: evidence for conservative behavior. Estuar. Coasts 37 (4), 1017–1027. https://doi.org/10.1007/s12237-013-9736-7.
Smith, G.I., Medrano, M.D., 1996. Continental borate deposits of Cenozoic age. In: Grew, E.S., Anovitz, L.M. (Eds.), Boron: Mineralogy, Petrology and Geochemistry. Mineral. Soc. Am.pp. 263–298.
Smith, M.P., Yardley, B.W.D., 1996. The boron isotopic composition of tourmaline as a guide to fluid processes in the southwestern England orefield: an ion microprobe study. Geochim. Cosmochim. Acta 60 (8), 1415–1427. https://doi.org/10.1016/0016-7037(96)00007-5.
Smith, H.J., Spivack, A.J., Staudigel, H., Hart, S.R., 1995. The boron isotopic composition of altered oceanic crust. Chem. Geol. 126 (2), 119–135. https://doi.org/10.1016/0009-2541(95)00113-6.
Spivack, A.J., 1986. Boron Isotope Geochemistry. Ph.D Thesis, MIT-WHOI Joint Program in Oceanography Cambridge, Massachusetts, USA.
Spivack, A.J., Edmond, J.M., 1987. Boron isotope exchange between seawater and the oceanic crust. Geochim. Cosmochim. Acta 51 (5), 1033–1043. https://doi.org/10.1016/0016-7037(87)90198-0.
Spivack, A.J., You, C.F., 1997. Boron isotopic geochemistry of carbonates and pore waters, Ocean Drilling Program Site 851. Earth Planet. Sci. Lett. 152 (1-4), 113–122. https://doi.org/10.1016/S0012-821x(97)00134-9.
Spivack, A.J., Palmer, M.R., Edmond, J.M., 1987. The sedimentary cycle of the boron isotopes. Geochim. Cosmochim. Acta 51 (7), 1939–1949. https://doi.org/10.1016/0016-7037(87)90183-9.
Spivack-Birndorf, L.J., Stewart, B.W., 2006. Use of boron isotopes to track the interaction of coal utilization byproducts with water in the environment. GSA, Abstr. Prog. 38 (7), 95.
Sullivan, P.L., Ma, L., West, N., Jin, L., Karwan, D.L., Noireaux, J., Steinhoefel, G., Gaines, K.P., Eissenstat, D.M., Gaillardet, J., Derry, L.A., Meek, K., Hynek, S., Brantley, S.L., 2016. CZ-tope at Susquehanna Shale Hills CZO: synthesizing multiple isotope proxies to elucidate Critical Zone processes across timescales in a temperate forested landscape. Chem. Geol. 445, 103–119. https://doi.org/10.1016/j.chemgeo.2016.05.012.
Sun, A.D., Xu, Q.C., Liu, L.H., Zhang, Y.L., Xu, S.J., 2014. Separation and analysis of boron and its isotopic composition in plants. Chin. J. Anal. Chem. 42 (1), 83–87. https://doi.org/10.3724/sp.j.1096.2014.30828.
Sun, A., Xu, Q., Wei, G., Zhu, H., Chen, X., 2018. Differentiation analysis of boron isotopic fractionation in different forms within plant organ samples. Phytochemistry 147, 9–13. https://doi.org/10.1016/j.phytochem.2017.12.012.
Swihart, G.H., Moore, B., Callis, E.L., 1986. Boron isotopic composition of marine and nonmarine evaporite borates. Geochim. Cosmochim. Acta 50 (6), 1297–1301. https://doi.org/10.1016/0016-7037(86)90413-8.
Swihart, G.H., McBay, E.H., Smith, D.H., Siefke, J.W., 1996. A boron isotopic study of a mineralogically zoned lacustrine borate deposit: the Kramer deposit, California, U.S.A. Chem. Geol. 127 (1), 241–250. https://doi.org/10.1016/0009-2541(95)00094-1.
Tanaka, R., Nakamura, E., 2005. Boron isotopic constraints on the source of Hawaiian shield lavas. Geochim. Cosmochim. Acta 69 (13), 3385–3399. https://doi.org/10.1016/j.gca.2005.03.009.
Thompson, A., Ruiz, J., Chadwick, O.A., Titus, M., Chorover, J., 2007. Rayleigh fractionation of iron isotopes during pedogenesis along a climate sequence of Hawaiian basalt. Chem. Geol. 238 (1–2), 72–83. https://doi.org/10.1016/j.chemgeo.2006.11.005.
Tipper, E.T., Lemarchand, E., Hindshaw, R.S., Reynolds, B.C., Bourdon, B., 2012. Seasonal sensitivity of weathering processes: hints from magnesium isotopes in a glacial stream. Chem. Geol. 312–313, 80–92. https://doi.org/10.1016/j.chemgeo.2012.04.002.
Tonarini, S., Pennisi, M., Leeman, W.P., 1997. Precise boron isotopic analysis of complex silicate (rock) samples using alkali carbonate fusion and ion-exchange separation. Chem. Geol. 142 (1-2), 129–137. https://doi.org/10.1016/S0009-2541(97)00087-9.
Tonarini, S., Leeman, W.P., Leat, P.T., 2011. Subduction erosion of forearc mantle wedge implicated in the genesis of the South Sandwich Island (SSI) arc: evidence from boron isotope systematics. Earth Planet. Sci. Lett. 301 (1-2), 275–284. https://doi.org/10.1016/j.epsl.2010.11.008.
Trumbull, R.B., Slack, J.F., 2018. Boron isotopes in the continental crust: granites, pegmatites, felsic volcanic rocks, and related ore deposits. In: Marschall, H., Foster, G. (Eds.), Boron Isotopes: The Fifth Element. Springer International Publishing, Cham, pp. 249–272.
Trumbull, R.B., Krienitz, M.S., Gottesmann, B., Wiedenbeck, M., 2008. Chemical and boron-isotope variations in tourmalines from an S-type granite and its source rocks: the Erongo granite and tourmalinites in the Damara Belt. Namibia. Contrib. Mineral. Petrol. 155 (1), 1–18. https://doi.org/10.1007/s00410-007-0227-3.
Trumbull, R.B., Beurlen, H., Wiedenbeck, M., Soares, D.R., 2013. The diversity of B-isotope variations in tourmaline from rare-element pegmatites in the Borborema Province of Brazil. Chem. Geol. 352, 47–62. https://doi.org/10.1016/j.chemgeo.2013.05.021.
Turner, S., Tonarini, S., Bindeman, I., Leeman, W.P., Schaefer, B.F., 2007. Boron and oxygen isotope evidence for recycling of subducted components over the past 2.5 Gyr. Nature 447 (7145), 702–705. https://doi.org/10.1038/nature05898.
Uchikawa, J., Penman, D.E., Zachos, J.C., Zeebe, R.E., 2015. Experimental evidence for kinetic effects on B/Ca in synthetic calcite: implications for potential $B(OH)_4^-$ and $B(OH)_3$ incorporation. Geochim. Cosmochim. Acta 150, 171–191. https://doi.org/10.1016/j.gca.2014.11.022.
Uppin, M., Karro, E., 2013. Determination of boron and fluoride sources in groundwater: batch dissolution of carbonate rocks in water. Geochem. J. 47 (5), 525–535. https://doi.org/10.2343/geochemj.2.0274.
Vengosh, A., Chivas, A.R., McCulloch, M.T., Starinsky, A., Kolodny, Y., 1991a. Boron isotope geochemistry of Australian salt lakes. Geochim. Cosmochim. Acta 55 (9), 2591–2606. https://doi.org/10.1016/0016-7037(91)90375-f.
Vengosh, A., Kolodny, Y., Starinsky, A., Chivas, A.R., Mcculloch, M.T., 1991b. Coprecipitation and isotopic fractionation of boron in modern biogenic carbonates. Geochim. Cosmochim. Acta 55 (10), 2901–2910. https://doi.org/10.1016/0016-7037(91)90455-E.
Vengosh, A., Starinsky, A., Kolodny, Y., Chivas, A.R., Raab, M., 1992. Boron isotope variations during fractional evaporation of sea water: new constraints on the marine vs. nonmarine debate. Geology 20 (9), 799–802. https://doi.org/10.1130/0091-7613(1992)020<0799:Bivdfe>2.3.Co;2.
Vengosh, A., Chivas, A.R., Starinsky, A., Kolodny, Y., Baozhen, Z., Pengxi, Z., 1995. Chemical and boron isotope compositions of non-marine brines from the Qaidam Basin, Qinghai, China. Chem. Geol. 120 (1-2), 135–154. https://doi.org/10.1016/0009-2541(94)00118-r.
Vils, F., Tonarini, S., Kalt, A., Seitz, H.M., 2009. Boron, lithium and strontium isotopes as tracers of seawater-serpentinite interaction at Mid-Atlantic ridge, ODP Leg 209. Earth Planet. Sci. Lett. 286 (3-4), 414–425. https://doi.org/10.1016/j.epsl.2009.07.005.
Voinot, A., Lemarchand, D., Collignon, C., Granet, M., Chabaux, F., Turpault, M.P., 2013. Experimental dissolution vs. transformation of micas under acidic soil conditions: clues from boron isotopes. Geochim. Cosmochim. Acta 117, 144–160. https://doi.org/10.1016/j.gca.2013.04.012.
Wang, Q.Z., Xiao, Y.K., Zhang, C.G., Wei, H.Z., Zhao, Z.Q., 2001. Boron isotopic compositions of some boron minerals in Qinghai and Tibet. Bull. Mineral. Petrol.

Geochem. 20 (4), 364–366.
Warner, N.R., Kresse, T.M., Hays, P.D., Down, A., Karr, J.D., Jackson, R.B., Vengosh, A., 2013. Geochemical and isotopic variations in shallow groundwater in areas of the Fayetteville Shale development, north-central Arkansas. Appl. Geochem. 35, 207–220. https://doi.org/10.1016/j.apgeochem.2013.04.013.
Warner, N.R., Darrah, T.H., Jackson, R.B., Millot, R., Kloppmann, W., Vengosh, A., 2014. New tracers identify hydraulic fracturing fluids and accidental releases from oil and gas operations. Environ. Sci. Technol. 48 (21), 12552–12560. https://doi.org/10.1021/es5032135.
Wedepohl, K.H., 1971. Environmental influences on the chemical composition of shales and clays. Phys. Chem. Earth 8, 305–333. https://doi.org/10.1016/0079-1946(71)90020-6.
Wei, G.J., Wei, J.X., Liu, Y., Ke, T., Ren, Z.Y., Ma, J.L., Xu, Y.G., 2013. Measurement on high-precision boron isotope of silicate materials by a single column purification method and MC-ICP-MS. J. Anal. At. Spectrom. 28 (4), 606–612. https://doi.org/10.1039/c3ja30333k.
Wei, H.Z., Jiang, S.Y., Tan, H.B., Zhang, W.J., Li, B.K., Yang, T.L., 2014a. Boron isotope geochemistry of salt sediments from the Dongtai salt lake in Qaidam Basin: boron budget and sources. Chem. Geol. 380, 74–83. https://doi.org/10.1016/j.chemgeo.2014.04.026.
Wei, H.Z., Jiang, S.Y., Yang, T.L., Yang, J.H., Yang, T., Yan, X., Ling, B.P., Liu, Q., Wu, H.P., 2014b. Effect of metasilicate matrices on boron purification by Amberlite IRA 743 boron specific resin and isotope analysis by MC-ICP-MS. J. Anal. At. Spectrom. 29 (11), 2104–2107. https://doi.org/10.1039/C4ja00153b.
West, A.J., Galy, A., Bickle, M., 2005. Tectonic and climatic controls on silicate weathering. Earth Planet. Sci. Lett. 235 (1-2), 211–228. https://doi.org/10.1016/j.epsl.2005.03.020.
Widory, D., Kloppmann, W., Chery, L., Bonnin, J., Rochdi, H., Guinamant, J.L., 2004. Nitrate in groundwater: an isotopic multi-tracer approach. J. Contam. Hydrol. 72 (1-4), 165–188. https://doi.org/10.1016/j.jconhyd.2003.10.010.
Widory, D., Petelet-Giraud, E., Negrel, P., Ladouche, B., 2005. Tracking the sources of nitrate in groundwater using coupled nitrogen and boron isotopes: a synthesis. Environ. Sci. Technol. 39 (2), 539–548. https://doi.org/10.1021/es0493897.
Widory, D., Petelet-Giraud, E., Brenot, A., Bronders, J., Tirez, K., Boeckx, P., 2013. Improving the management of nitrate pollution in water by the use of isotope monitoring: the $\delta^{15}N$, $\delta^{18}O$ and $\delta^{11}B$ triptych. Isot. Environ. Health Stud. 49 (1), 29–47. https://doi.org/10.1080/10256016.2012.666540.
Wieser, M.E., Iyer, S.S., Krouse, H.R., Cantagallo, M.I., 2001. Variations in the boron isotope composition of Coffea arabica beans. Appl. Geochem. 16 (3), 317–322. https://doi.org/10.1016/s0883-2927(00)00031-7.
Williams, L.B., Hervig, R.L., 2002. Exploring intra-crystalline B-isotope variations in mixed-layer illite-smectite. Am. Mineral. 87 (11-12), 1564–1570. https://doi.org/10.2138/am-2002-11-1206.
Williams, L.B., Hervig, R.L., 2004. Boron isotope composition of coals: a potential tracer of organic contaminated fluids. Appl. Geochem. 19 (10), 1625–1636. https://doi.org/10.1016/j.apgeochem.2004.02.007.
Williams, L.B., Hervig, R.L., Holloway, J.R., Hutcheon, I., 2001a. Boron isotope geochemistry during diagenesis. Part I. Experimental determination of fractionation during illitization of smectite. Geochim. Cosmochim. Acta 65 (11), 1769–1782. https://doi.org/10.1016/s0016-7037(01)00557-9.
Williams, L.B., Hervig, R.L., Hutcheon, I., 2001b. Boron isotope geochemistry during diagenesis. Part II. Applications to organic-rich sediments. Geochim. Cosmochim. Acta 65 (11), 1783–1794. https://doi.org/10.1016/s0016-7037(01)00558-0.
Williams, L.B., Hervig, R.L., Wieser, M.E., Hutcheon, I., 2001c. The influence of organic matter on the boron isotope geochemistry of the gulf coast sedimentary basin, USA. Chem. Geol. 174 (4), 445–461. https://doi.org/10.1016/s0009-2541(00)00289-8.
Williams, L.B., Turner, A., Hervig, R.L., 2007. Intracrystalline boron isotope partitioning in illite-smectite: testing the geothermometer. Am. Mineral. 92 (11-12), 1958–1965. https://doi.org/10.2138/am.2007.2531.
Williams, L.B., Środoń, J., Huff, W.D., Clauer, N., Hervig, R.L., 2013. Light element distributions (N, B, Li) in Baltic Basin bentonites record organic sources. Geochim. Cosmochim. Acta 120, 582–599. https://doi.org/10.1016/j.gca.2013.07.004.
Winter, J.D., 2014. Principles of Igneous and Metamorphic Petrology. Pearson Higher, USA.
Woodford, D.T., Sisson, V.B., Leeman, W.P., 2001. Boron metasomatism of the Alta stock contact aureole, Utah: evidence from berates, mineral chemistry, and geochemistry. Am. Mineral. 86 (4), 513–533. https://doi.org/10.2138/am-2001-0415.
Wunder, B., Meixner, A., Romer, R.L., Wirth, R., Heinrich, W., 2005. The geochemical cycle of boron: constraints from boron isotope partitioning experiments between mica and fluid. Lithos 84 (3-4), 206–216. https://doi.org/10.1016/j.lithos.2005.02.003.
Xiao, Y.K., Wang, L., 2001. The effect of pH and temperature on the isotopic fractionation of boron between saline brine and sediments. Chem. Geol. 171 (3-4), 253–261. https://doi.org/10.1016/S0009-2541(00)00251-5.
Xiao, Y.K., Beary, E.S., Fassett, J.D., 1988. An improved method for the high-precision isotopic measurement of boron by thermal ionization mass-spectrometry. Int. J. Mass Spectrom. Ion Process. 85 (2), 203–213. https://doi.org/10.1016/0168-1176(88)83016-7.
Xiao, Y.K., Sun, D.P., Wang, Y.H., Qi, H.P., Jin, L., 1992. Boron isotopic compositions of brine, sediments, and source water in Da Qaidam Lake, Qinghai, China. Geochim. Cosmochim. Acta 56 (4), 1561–1568. https://doi.org/10.1016/0016-7037(92)90225-8.
Xiao, Y.K., Shirodkar, P.V., Liu, W.G., Sun, D.P., Wang, Y.H., Jin, L., 1999. Boron isotopic geochemistry of salt lakes, Qaidam Basin, China. Advance of Nature Science 917, 612–618 (in Chinese).
Xiao, Y.K., Li, S.Z., Wei, H.Z., Sun, A.D., Liu, W.G., Zhou, W.J., Zhao, Z.Q., Liu, C.Q., Swihart, G.H., 2007. Boron isotopic fractionation during seawater evaporation. Mar. Chem. 103 (3-4), 382–392. https://doi.org/10.1016/j.marchem.2006.10.007.
Xiao, Y.K., Li, H.L., Liu, W.G., Wang, X.F., Jiang, S.Y., 2008. Boron isotopic fractionation in laboratory inorganic carbonate precipitation: evidence for the incorporation of B$(OH)_3$ into carbonate. Sci. China. Ser. D Earth Sci. 51 (12), 1776–1785. https://doi.org/10.1007/s11430-008-0144-y.
Xiao, J., Xiao, Y.K., Jin, Z.D., He, M.Y., Liu, C.Q., 2013. Boron isotope variations and its geochemical application in nature. Aust. J. Earth Sci. 60 (4), 431–447. https://doi.org/10.1080/08120099.2013.813585.
Xu, Q., Dong, Y., Zhu, H., Sun, A., 2015. Separation and analysis of boron isotope in high plant by thermal ionization mass spectrometry. Int. J. Anal. Chem. 2015, 6. https://doi.org/10.1155/2015/364242.
You, C.F., Spivack, A.J., Gieskes, J.M., Martin, J.B., Davisson, M.L., 1996. Boron contents and isotopic compositions in pore waters: a new approach to determine temperature induced artifacts – geochemical implications. Mar. Geol. 129 (3-4), 351–361. https://doi.org/10.1016/0025-3227(96)83353-6.
Yuan, J.F., Guo, Q.H., Wang, Y.X., 2014. Geochemical behaviors of boron and its isotopes in aqueous environment of the Yangbajing and Yangyi geothermal fields, Tibet, China. J. Geochem. Explor. 140, 11–22. https://doi.org/10.1016/j.gexplo.2014.01.006.
Zhang, S., Henehan, M.J., Hull, P.M., Reid, R.P., Hardisty, D.S., Hood, A.v.S., Planavsky, N.J., 2017. Investigating controls on boron isotope ratios in shallow marine carbonates. Earth Planet. Sci. Lett. 458, 380–393. https://doi.org/10.1016/j.epsl.2016.10.059.
Zhao, Z.Q., Liu, C.Q., 2010. Anthropogenic inputs of boron into urban atmosphere: evidence from boron isotopes of precipitations in Guiyang City, China. Atmos. Environ. 44 (34), 4165–4171. https://doi.org/10.1016/j.atmosenv.2010.07.035.
Zhao, K.D., Jiang, S.Y., Nakamura, E., Moriguti, T., Palmer, M.R., Yang, S.Y., Dai, B.Z., Jiang, Y.H., 2011. Fluid-rock interaction in the Qitianling granite and associated tin deposits, South China: evidence from boron and oxygen isotopes. Ore Geol. Rev. 43 (1), 243–248. https://doi.org/10.1016/j.oregeorev.2011.07.002.
Zhao, K.D., Jiang, S.Y., Nakamura, E., Moriguti, T., Wet, H.Z., 2015. A preliminary study on boron isotope fractionation of major rock-forming minerals in granite. Acta Petrol. Sin. 31 (3), 740–746.
Zheng, M., Liu, X., 2009. Hydrochemistry of salt lakes of the Qinghai-Tibet Plateau, China. Aquat. Geochem. 15 (1), 293–320. https://doi.org/10.1007/s10498-008-9055-y.